CLIMATE CHANGE SCENARIOS FOR MALAYSIA 2001 - 2099

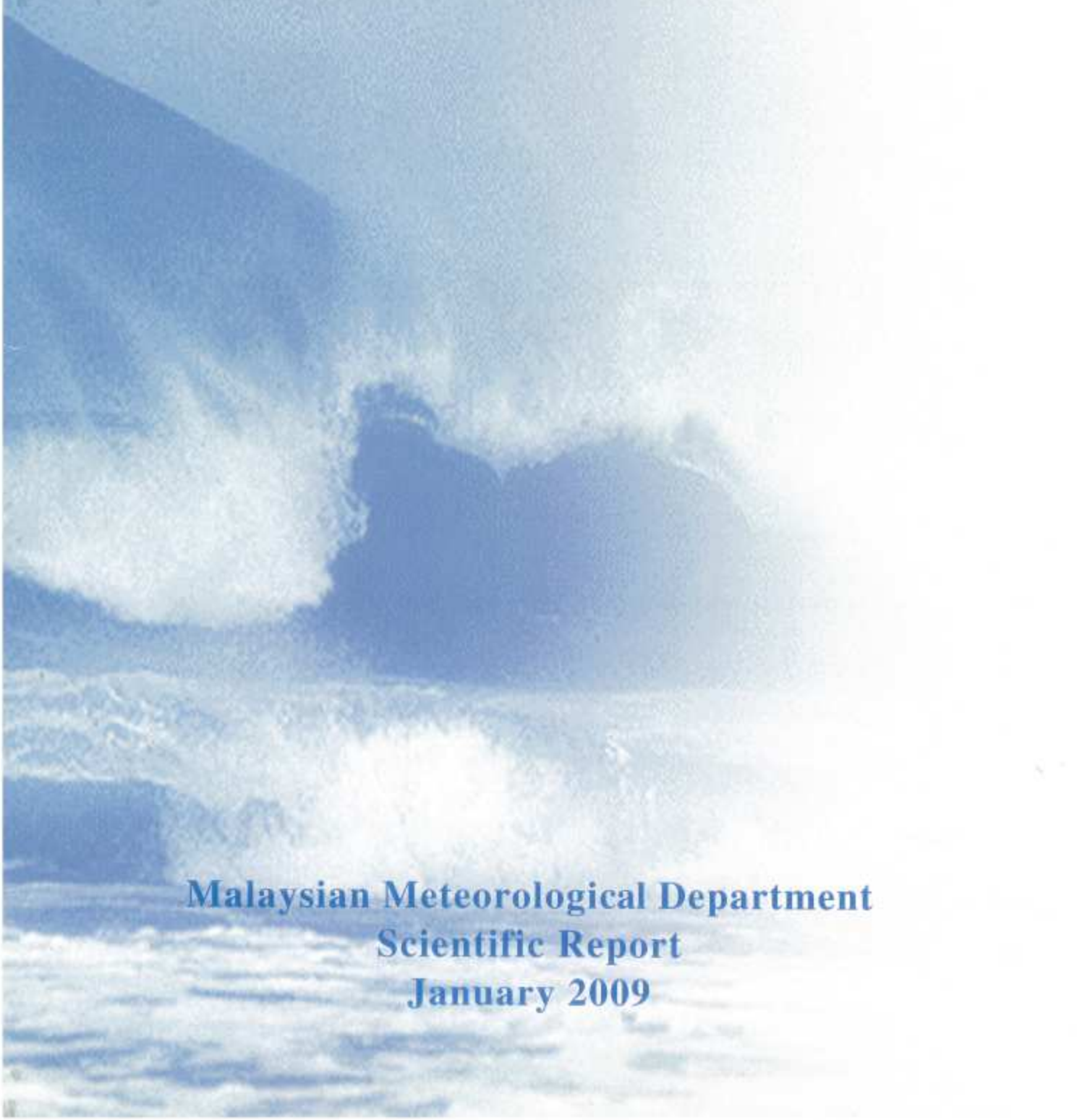

Malaysian Meteorological Department
Scientific Report
January 2009

ISBN 978-983-99679-1-3

CLIMATE CHANGE SCENARIOS FOR MALAYSIA 2001 - 2099

Malaysian Meteorological Department

Scientific Report

January 2009

Prepared by:

Numerical Weather Prediction Development Section

Technical Development Division

Malaysian Meteorological Department

Ministry of Science, Technology and Innovation

Executive Summary

Earth surface temperature records have clearly indicated that the climate of the earth is warming. The Intergovernmental Panel on Climate Change (IPCC) Fourth Assessment Report (AR4) has come with a 0.74 °C increase in global average surface temperature for the past 100 years based upon past IPCC assessments and new findings reported in researches carried out during the last 6 years. This unprecedented increase is primarily due to increasing concentration of greenhouse gases (GHG) in the atmosphere. The AR4 also indicates that extreme rainfall events have increased over most land areas, consistent with warming and increase of atmospheric water vapor.

Different emission scenarios describe the different rates of GHG emissions into the atmosphere. Global and regional climate models capture the climate response to these different scenarios. A2, A1B and B2 emission scenarios are considered for the regional climate simulation. Only the A1B is considered for the global climate simulation. It was found that Carbon dioxide emission rates are more than double in A2 scenario as compared to A1B and B2 scenarios towards the end of the century.

Present regional climatic trends are in line with the increase in average surface temperature observed for Malaysia. Nevertheless rainfall trends for Malaysia are not clearly defined as this parameter has large spatial and temporal variation. Significant regional temperature increase is very much correlated to the El Niño events. Higher regional temperature increase is indicated for Peninsular Malaysia compared to East Malaysia, with western Peninsular Malaysia region experiencing the highest increase.

The frequency of relatively drier years has increased for Peninsular Malaysia and East Malaysia as of 1970. Most of the El Niño events as of 1970 have resulted in relatively drier years for Peninsular Malaysia and East Malaysia. Most of the severe dry spells in East Malaysia have been recorded during the El Niño events. Though the three driest years for Peninsular Malaysia (1963, 1997 and 2002) were recorded during El Niño events, the substantial

frequency of relatively dry years in Peninsular Malaysia not accounted for by El Niño event indicates that El Niño event on its own is not the primary rainfall regulatory mechanism for Peninsular Malaysia.

Climate simulations for the Malaysian region have been studied using twelve coupled Atmosphere-Ocean General Circulation Models (AOGCMs). An ensemble mean for temperature and rainfall was obtained using nine out of twelve AOGCMs, which were based upon the A1B scenario. The ensemble result indicates an increasing temperature trend for the 3 domains, Peninsular Malaysia, Sabah and Sarawak. Temperature and rainfall anomalies were obtained by comparing future projection values with the average values obtained for the last decade of the 20th century (1990 – 1999). The projected temperature increase among the nine AOGCMs for East Malaysia and Peninsular Malaysia are 1.0°C to 3.5°C and 1.1°C to 3.6°C respectively. The ensemble rainfall is projected to increase most significantly in western Sarawak in comparison with other regions in Malaysia. Rainfall over the western Peninsular Malaysia is projected to increase while there is reduction projected for eastern Peninsular Malaysia.

The Northeast Monsoon circulation during the months of December, January and February for Asia was also analyzed based on the 9 AOGCMs. This is the period during which most of the flooding in Malaysia occurs. During this period the strong northeasterly and easterly winds flow from the western Pacific into the South China Sea is a prominent feature. The strength of these winds influences the rainfall intensity over Malaysia during the winter monsoon.

A projection of the Winter Monsoon Intensity Index is used to gauge the projected intensity of the Northeast Monsoon during the 21st century. The interannual variation of the Winter Monsoon Intensity Index is closely related to the tropical Pacific sea surface temperature (SST) anomaly. This suggests that processes associated with the SST anomaly over the tropical Pacific mainly influence the strength of the Northeast Monsoon. The winter monsoon generally becomes weaker during an El Niño event and stronger during a La

Niña event. The projected 850hPa wind circulation pattern anomaly and the negative trends in the ensemble projection of the Winter Monsoon Intensity Index indicate an overall weakening of the East Asian Winter Monsoon and therefore the impact of the Northeast Monsoon in regard to South East Asia.

Given the coarse resolution of GCM simulations, Regional Climate Models (RCMs) are used to simulate localized forcings such as elevated topography and coastlines upon lateral boundary data from various AOGCMs and Atmospheric Global Circulation Models (AGCMs). This enables the Regional Climate Model (RCM) to be able to provide high-resolution information on a large physically consistent set of climate variables and therefore better represent extreme events. The regional climate-modelling tool used in the Malaysian Meteorological Department is the Providing Regional Climates for Impacts Studies (PRECIS) model developed by the Hadley Center, United Kingdom. Observational data from the Climate Research Unit of the University of East Anglia, United Kingdom was used to validate the baseline (1961 – 1990) regional climate simulation. The monthly temperature variation pattern and rainfall distribution simulated by the PRECIS RCM is consistent with the observational data.

Annual average surface temperature increase consistent with the GCM signal was obtained for Peninsular Malaysia, Sabah and Sarawak. Nevertheless regional modelling did simulate a deviation from the GCM in regard to projected temperatures for the period of 2080 to 2089. A significant reduction of 0.4°C to 0.5°C in RCM projected annual average surface temperature was obtained for all the three sub regions during the 2080 to 2089 decade. The annual average surface temperature trends for all the three sub regions are quite consistent. Projected seasonal temperature increase is quite consistent among Peninsular Malaysia, Sabah and Sarawak throughout the four different seasons with exception of March – April - May. During this season Sabah shows markedly higher annual average temperature increase compared to Peninsular Malaysia and Sarawak.

Significant annual average temperature increase with record high temperatures is simulated for all three regions for the years 2028, 2048, 2061 and 2079. Highest and lowest projected seasonal average temperature towards the end of the century for Peninsular Malaysia is obtained during DJF (3.7°C) and SON (3.3°C) respectively. For Sabah the highest and lowest projected increase is obtained during MAM (4.1°C) and SON (3.2°C) respectively. For Sarawak, the highest and lowest projected increase is obtained during MAM (3.9°C) and DJF (3.4°C). Analyzing the projected temperatures for the three emission scenarios, A2, A1B and B2, the annual average surface temperature increase range between the lowest value (indicated by the B2 simulation) and the highest value (indicated by the A2 simulation) is 2.3°C to 3.6°C for Peninsular Malaysia and 2.4°C to 3.7°C for East Malaysia.

Generally the PRECIS RCM driven by the HadCM3 A1B emission scenario has simulated a reduction in regional annual average rainfall for Malaysia. The negative annual rainfall trend is far more evident in Sabah compared to Peninsular Malaysia and Sarawak. The significant increase in annual temperature simulated for 2028, 2048, 2061 and 2079 is consistent with the corresponding significant reduction in annual average rainfall projected for the same four years mentioned above. This consistent significant reduction of rainfall together with significant increase in temperature is generally exhibited during El Niño events. In the case of the four years mentioned above, Peninsular Malaysia, Sabah and Sarawak are all affected, which is a signature of a strong El Niño. The impact of El Niño and La Niña events are more significant in East Malaysia compared to Peninsular Malaysia.

Projection of an increasing seasonal rainfall pattern is simulated for all the three sub regions during the last 20 years of the simulation period (2079 – 2099). This holds true for all the four seasons. Projection of seasonal temporal rainfall variation is largest (-60% to 40%) during the months of December, January and February. Meanwhile projection of seasonal temporal rainfall variation is minimal (-15% to 25%) during the months of September, October and November. Lower annual average rainfall projection for

Peninsular Malaysia, Sabah and Sarawak is indicated comparing the B2 scenario and A2 scenario. A significant departure between the A1B emission scenario and the A2 and B2 emission scenarios is obtained around 2082 to 2093. An evident upward trend of annual rainfall is simulated for the A1B scenario, but a downward trend is projected for both the A2 and B2 scenarios. Reduction in average annual rainfall projected for the A2 and B2 scenarios is more severe in Sabah and Sarawak compared to Peninsular Malaysia.

A more spatially detailed regional analysis of the temperature simulation reveals that towards the end of the century, highest temperatures are simulated for Eastern Sarawak sub region (3.8°C) and lowest values for North-eastern Peninsular Malaysia. The rate of temperature increase for all sub regions considered during the 30-year period from 2059 to 2090 is generally double the rate of increase simulated for earlier 20-year period from 2029 to 2050. Rainfall simulation reveals that the PRECIS RCM simulates more rainfall during 2090 – 2099 for the whole country compared to 2020 – 2029 and 2050 – 2059. During 2090 – 2099, higher rainfall is simulated in Peninsular Malaysia compared to East Malaysia. The PRECIS RCM also simulates higher amount of rainfall over land areas compared to the South China Sea. At the sub regional scale, towards the end of the century, highest rainfall is simulated for Southern Peninsular Malaysia. Least rainfall is simulated during the same period for East Sabah.

Uncertainties are inherent in RCMs and GCMs. Although it is very difficult to quantify all the aspects of these uncertainties, it is necessary to consider these uncertainties when impacts, vulnerability and adaptation options are being assessed. Primary source of uncertainties are the future emission scenarios, the future atmospheric greenhouse gas concentrations, incomplete understanding of the global and regional climate systems, pattern-scaling methods and natural variability.

Acknowledgements

We would like to express our gratitude to the Hadley Centre, United Kingdom in regard to their invaluable support. The Regional Climate Model PRECIS used in the Malaysian Meteorological Department was obtained from the Hadley Centre in August 2006. Subsequently continued support in regard to lateral boundary data supply and software upgrade has always been provided continuously. Immense help have been rendered in regard to trouble shooting problems encountered while running the regional climate model.

Grateful appreciation is extended to the Director General of the Malaysian Meteorological Department for his encouragement to undertake this study. We would also like to thank the Climate and Hydrology Division of the Malaysian Meteorological Department for making available images depicting the current and historical climate representation for Peninsular Malaysia and East Malaysia.

CONTENTS

Chapter 1: Global Warming and Greenhouse Gas Emissions

1.1 Global Climate

Some aspects of the changing world climate such as sea level rise, non-polar glacial retreat and increased reduction of Artic sea ice extent and thickness during summer are indications of global warming. Nevertheless the global averaged surface temperature is the parameter that most clearly defines global warming.

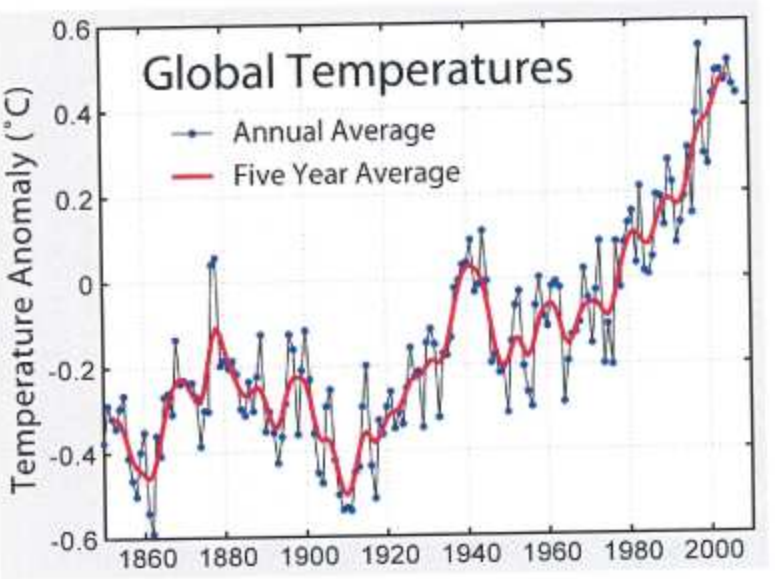

Figure 1: Global Averaged Surface Temperature (IPCC AR4 WG1: Physical Science Basis)

Figure 1 denotes the annual average and the corresponding five-year average for the global averaged surface temperature from 1860 to 2007. This data is a combination of surface air temperature over land and sea surface temperatures over the oceans. Based upon the Intergovernmental Panel on Climate Change (IPCC) Fourth Assessment Report (AR4), global temperatures have risen by about 0.74 °C since the beginning of the 20th century. This is up from the 0.6 °C increase in the 100 years prior to the IPCC Third Assessment Report (TAR). The single warmest year during the 147-

year period was 1998. Twelve of the thirteen years in the period (1995-2007) rank among the top 12 warmest years in the observation record.

Other aspects of climate change observations as given in the Working Group 1 Summary for Policymakers (SPM) of the Intergovernmental Panel on Climate Change (IPCC) Fourth Assessment Report are given below. Cold days and cold nights have become less frequent, while hot days, hot nights and heat waves have become more frequent. Frequency of heavy precipitation events has increased over most land areas, consistent with warming and observed increases of atmospheric water vapour. Since 1961 the ocean has been absorbing more than 80% of the heat added to the climate system, and ocean temperatures have increased to depths of at least 3000 m (9800 ft). Expansion of seawater due to this warming has resulted in sea level rise at an average rate of about 1.8 mm/year during the years 1961-2003. The rise in sea level during 1993-2003 was at an average rate of 3.1 mm/year. Nevertheless it is not clear whether this is a long-term trend or just variability. Losses from the land-based ice-sheets of Greenland and Antarctica have very likely contributed to sea level rise between 1993 and 2003.

Causes of global warming are generally categorized into natural and anthropogenic forcing. Natural forcing such as the tilt of the earth axis have time scales of thousands of years and variation in interaction between the ocean and atmosphere can result in climate variations of yearly, decadal and century time scales. Nevertheless simulation of historical global climate has shown that natural forcings alone could not replicate the warming observed over the last 40 to 50 years. Only when both the natural and anthropogenic forcings were put together, could global simulations reproduce approximately the observed global warming.

Anthropogenic forcings are due to human induced activities which increase concentration of greenhouse gases (GHG) into the atmosphere. Carbon dioxide released from burning of fossil fuel and deforestation, methane emissions from agriculture activities and tropospheric ozone from vehicle

exhausts are effective in trapping of heat in the troposphere. In contrast aerosols such as sulphates due to sulphur dioxide emitted from fossil fuel burning brings in a cooling effect to the lower atmosphere.

1.2 Greenhouse Gas Emissions

Human economic activities have caused the greenhouse gas (GHG) emissions. Different emission scenarios will produce different rate of GHG emissions. Based on these different emission scenarios, global and regional climate models are used to project the future climate. The IPCC Special Report on Emission Scenarios (SRES) has described four main emission marker scenarios based on the assumptions on how the world population, economy, energy-technology and life style will evolve. They are known as **A1**, **A2**, **B1** and **B2** emission scenarios. The details of these emission scenarios are summarized in **Appendix 1**.

Simulation of future climate requires assumptions on the future atmospheric concentrations of GHG and aerosols. Inclusion of the aerosols are necessary, especially sulphate aerosols, as they have a cooling effect in the lower atmosphere by scatter back sunlight and change the properties of clouds.

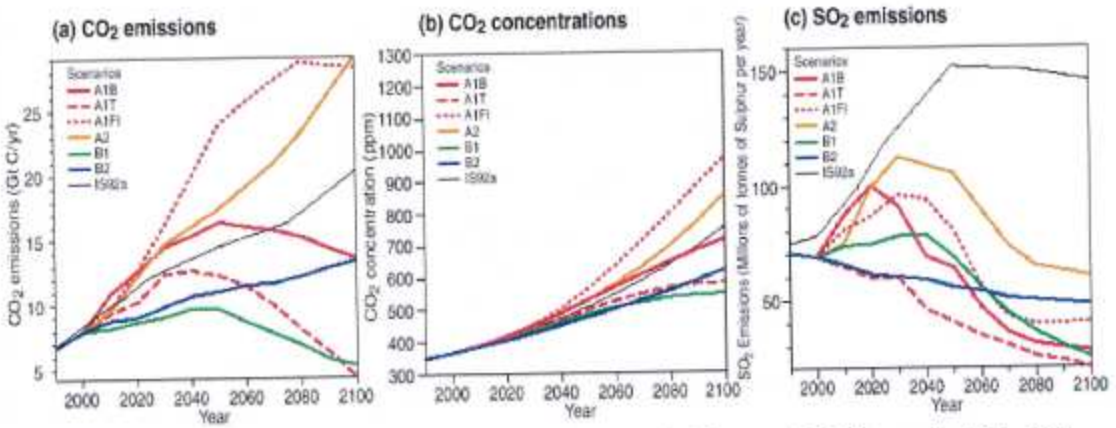

Figure 2: Future Emissions and Concentrations of CO_2 and SO_2 for Different Emissions Scenarios (Special Report on Emission Scenarios, 2000)

Global climate simulations were used to project the climate scenarios till the end of the century. **Figure 2** shows the future emissions of carbon dioxide and sulfur dioxide and atmospheric concentration of carbon dioxide for the various emission scenarios. It was found that carbon dioxide emission rates are more than double in A2 scenario compared to that of B2 and A1B scenarios towards the end of the century. The A1B scenario reflects continued practise of present day standards in regard to fuel type usage and socioeconomic activities. The carbon dioxide concentration towards the end of the century for the A1B scenario doubles the amount present in the beginning of the century that is from 350ppm to 700ppm. Emission rates of sulphur dioxide for most emission scenarios decrease after the mid of the century. Therefore given the long lifetime (~100 years) of carbon dioxide in the atmosphere, the global surface temperature is expected to continue increasing.

1.3 Climate Response

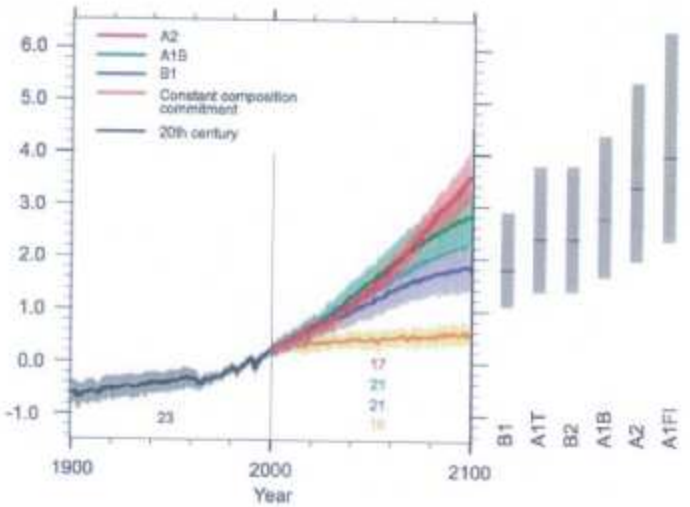

Figure 3: Annual Global Average Surface Air Temperature Increase From 1900 to 2100 for Different Emission Scenarios (IPCC AR4 WG1: Summary for Policy Makers)

Responses of the climate system to various emission scenarios are as shown in **Figure 3**. Although there are vast differences between the various emission scenarios (from minimal reliance on fossil fuel in B1 to total reliance on fossil fuel in A1F1), the difference in surface air temperature increase begins to diverge only after the middle of the century. This is because climate change for the next 30 to 40 years is greatly influence by past emissions. It may also be partially due to sulphate aerosols and GHG initially offsetting each other. The latter reason will become less important in the future as sulphate aerosol concentration in the atmosphere (**Figure 2c**) will reduce due to the decreasing tendency of fossil fuel usage. The warming rates between the various emission scenarios begin to diverge after 2050. By 2100, the warming simulated with respect to the 1961 to 1990 average, ranges from 1.9°C for the B1 emission scenario to 4.0°C for the A1F1 emission scenario.

The A1B emission scenario multi model simulation in comparison with 1980-1999 baseline as shown in **Figure 4** displays the regional climate change responses. Heating is more pronounced over the land compared to the oceans. The highest warming (more than 6°C) is noticed in the extreme northern latitudes. Comparatively land areas in the equatorial belt seem to be subjected to the least warming. No regions of the globe experiences cooling.

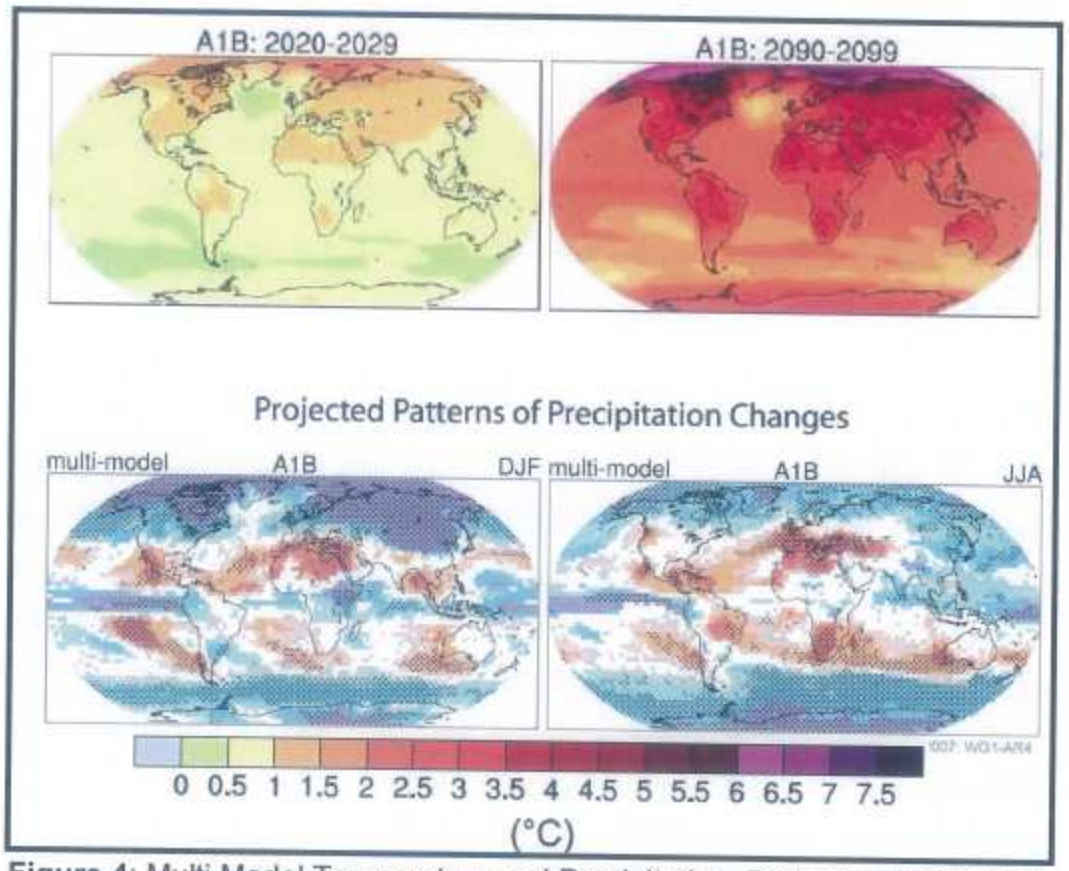

Figure 4: Multi Model Temperature and Precipitation Projection (IPCC AR4 WG1: Physical Science Basis)

Though global precipitation is supposed to increase due to higher amount of moisture in the atmosphere as a result of global warming, changes in spatial distribution of precipitation is more complex and less consistent between climate models. Precipitation anomaly for both the boreal winter (December-January-February or DJF) and summer seasons (June-July-August or JJA) are also shown in **Figure 4**. The increased precipitation pattern in the high latitudes of both the hemispheres is quite consistent in most climate models. This pattern is more pronounced during the boreal winter season. Prominent drying is experienced in Central America, Northern Africa, Western Australia, Southern Europe, South-Western United States, South–East Pacific and the Atlantic Ocean in general.

Chapter 2: Trends in Regional Climatology

2.1 Climate Trends of Southeast Asia

Southeast Asia is characterized by tropical rainforest and monsoon climates with high and constant precipitation (rainfall). Large portions of the region are made up of maritime continents with varied topographical scales. Therefore, the mountains and the complex land-sea configuration strongly influence the weather and climate of the region.

The climate of Southeast Asia is dominated by the two monsoons: The summer Southwest Monsoon influences the climate of the region from May to September, and the winter Northeast Monsoon from November to February. Tropical cyclones also play an important role with respect to the regional rainfall, especially during the Southwest Monsoon. Philippines and Vietnam are the main countries affected by cyclogenesis activity originating from the North-Western Pacific. Tropical storms and depressions are native to the South China Sea and the Indian Ocean sector of Southeast Asia.

Present climate trends in Southeast Asia have been characterised by increasing surface air temperature. Intraseasonal and interannual variability in regional rainfall trend has been observed over the past few decades. The El Niño-Southern Oscillation (ENSO), time scale based oscillation of the Indian Ocean Dipole (IOD) and the intraseasonal Madden Julian Oscillation (MJO) may influence extensively the observed interannual and intraseasonal rainfall distribution in Southeast Asia. Recent studies indicating the increased frequency and intensity of tropical cyclones originating in the Pacific, has had a major impact particularly on the Philippines and Vietnam.

Increasing intensity and spread of forest fires in Southeast Asia, which were observed in the past 20 years, are largely attributed to the rise in temperature and decline in rainfall in combination with increasing intensity of land-use. Fires in peat lands of Indonesia during the 1997 to 1998 El Niño dry season affected over 2 million hectares of land and emitted an estimated 0.81 to 2.57

PgC (1 PgC = 10^{15} g of Carbon) to the atmosphere. In the past 10 years about 3 million hectares of peat lands in Southeast Asia have been burnt, releasing between 3 to 5 PgC, and the drainage of peat land has affected an additional 6 million hectares and released a further 1 to 2 PgC (Page et al, 2002).

2.2 Past Climate Trends

The climate of Malaysia is tropical and humid. It is very much influenced by the mountainous topography and complex land-sea interactions. Intraseasonal and interdecadal fluctuations such as the ENSO, IOD and MJO are known to significantly influence the interannual climate variability of Malaysia. Increase in tropical storms in the South China Sea have contributed to more extreme events of rainfall and gusting in both East and West Malaysia. Annual trend analysis of both temperature and rainfall has been carried out by analyzing both the temperature and rainfall data for Malaysia over the last 40 years (1968-2007).

2.2.1 Temperature Analysis

The Kuching, Kota Kinabalu, Kuantan and Petaling Jaya meteorological stations were selected to represent Sarawak, Sabah, East Peninsular Malaysia and West Peninsular Malaysia respectively. The temperature trends for the 4 meteorological stations which represent the 4 different geographical locations were plotted as shown in **Figure 5**. Forty years climatic data will be able to capture more than 80% of the climate variation for a given region.

All the four stations indicate an increasing temperature trend. Kuching shows the least increase among the four stations. This may be due to the relatively larger areas of forest cover in Sarawak and the slower pace of urban development experienced. Nevertheless, it indicates consistent significant temporal variation in annual mean temperatures for all the regions. The significant years concerned are clearly shown in **Figure 5**. For most stations, new surface temperature maximum were recorded in 1972, 1982 and 1997.

From 1970 to 2004, strong El Niño events were recorded in 1972, 1982, 1987, 1991 and 1997. During these 5 years, all the four stations recorded significant annual temperature maximum. Western Peninsular Malaysia and Sabah show higher recorded temperatures than Eastern Peninsular Malaysia and Sarawak.

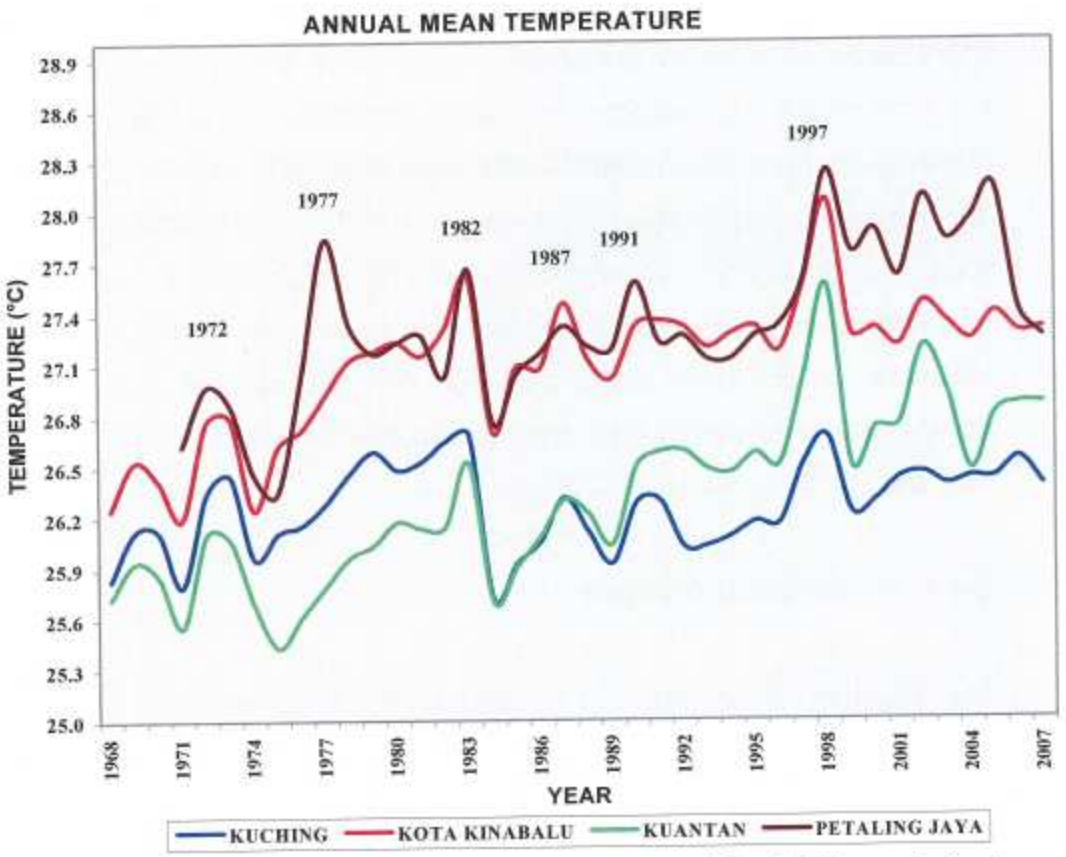

Figure 5: Annual Mean Temperature Trend for 4 Meteorological Stations

Figure 6 and **Figure 7** show the seasonal mean temperatures for Peninsular Malaysia and East Malaysia respectively. The analysis is divided into 4 seasons, December-January-February (DJF), March-April-May (MAM), June-July-August (JJA) and September-October-November (SON). The 1998-2007 10-year mean temperature was compared with 1961-1990 30-year mean temperature for Peninsular Malaysia and East Malaysia.

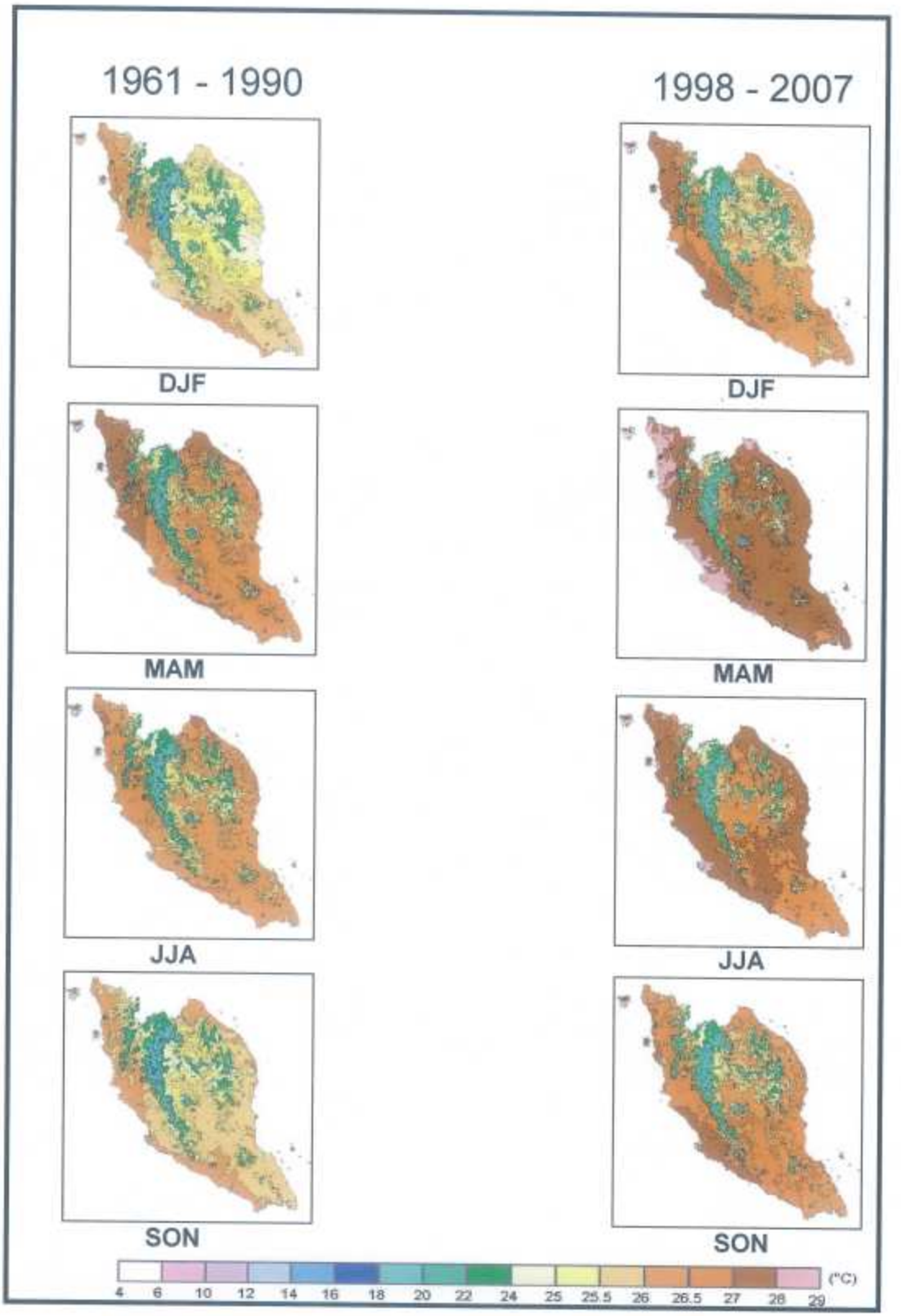

Figure 6: Long Term Mean Temperature for West Malaysia

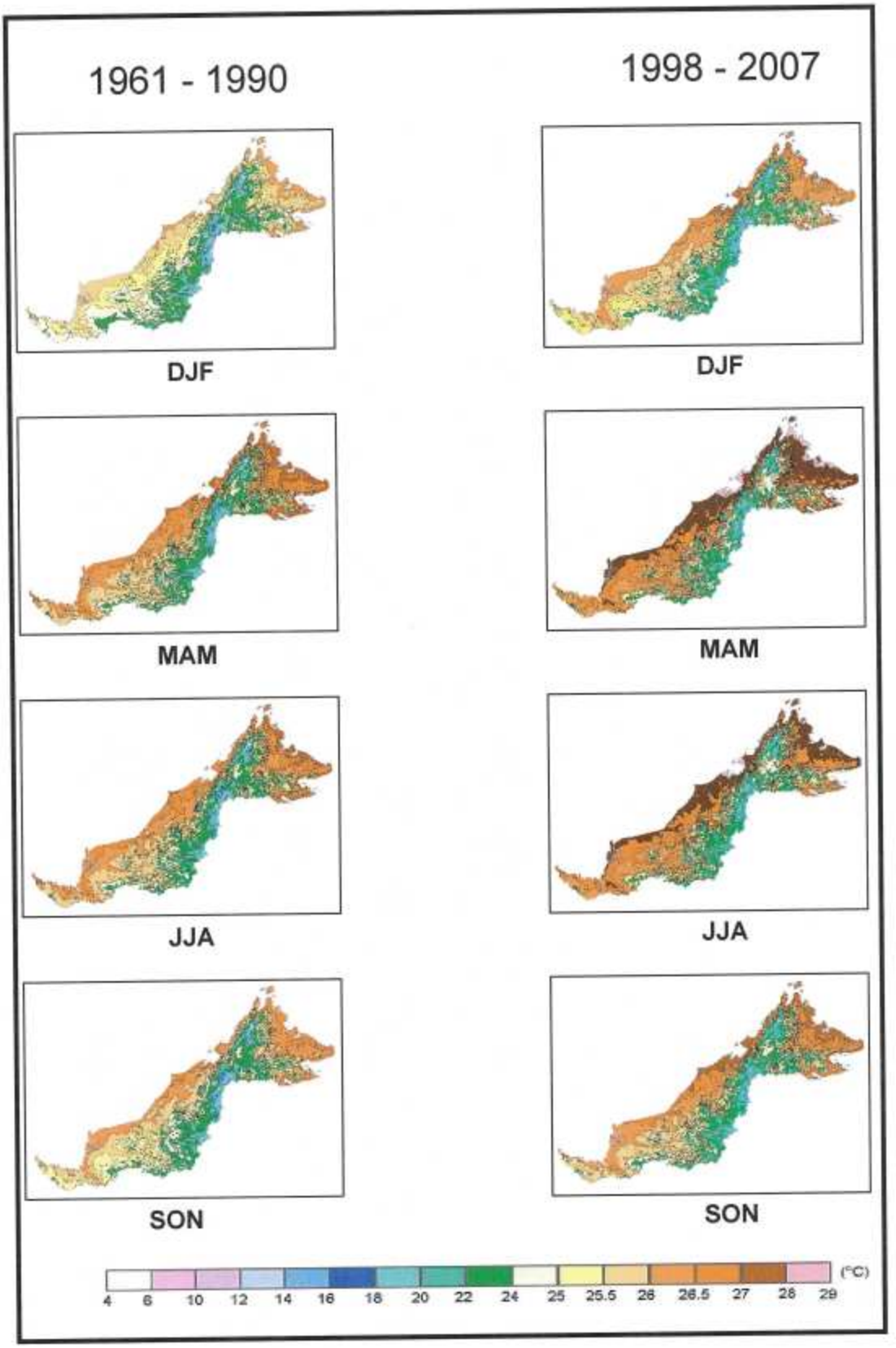

Figure 7: Long Term Mean Temperature for East Malaysia

For Peninsular Malaysia, MAM and DJF are the warmest and the coldest seasons respectively in 1961-1990 and 1998-2007 (**Figure 6**). For East Malaysia, DJF is the coldest season in both 1961-1990 and 1998-2007 (**Figure 7**). There is no significant difference between MAM and JJA to ascertain the difference among them in 1961-1990 (**Figure 7**). However in 1998-2007, MAM record higher mean temperatures than JJA.

Higher temperature increases are recorded in Peninsular Malaysia compared to East Malaysia when comparing the long term means obtained for 1961-1990 and 1998-2007. An average temperature increase of 0.5°C to 1.5°C is recorded in Peninsular Malaysia and 0.5°C to 1.0°C in East Malaysia. Western Peninsular Malaysia experiences more significant rise in temperature when compared to other regions in Malaysia. Among the four seasons, SON records the highest temperature increase for Peninsular Malaysia, followed by DJF. Nevertheless, for East Malaysia, temperature increase for all the seasons are about similar.

2.2.2 Rainfall Analysis

The spatial variability of rainfall lacks the regularity that is generally found with temperature. Therefore the standardized rainfall anomaly averaged for Peninsular Malaysia and East Malaysia is used to analyze the rainfall pattern for Malaysia. **Figures 8** and **9** show the standardized rainfall anomaly for Peninsular Malaysia and East Malaysia respectively. This standardized anomaly was obtained by normalizing the annual rainfall anomaly with the standard deviation of the total period considered. Meteorological stations data from 1951 to 2005 was used for this purpose. The El Niño and La Niña occurrences during this period are also indicated to better understand the impact of these events on the rainfall patterns of Malaysia.

In Peninsular Malaysia, reduction in rainfall is recorded for the second half of the period considered above. Dry years observed from 1975 to 2005 are more frequent and intense as compared to those of 1951 to 1975 (**Figure 8**). Most

of the El Niño events as of 1970 have resulted in severely dry years for Peninsular Malaysia. The three driest years for Peninsular Malaysia (1963, 1997 and 2002) have been recorded during El Niño events. Nevertheless, the El Niño phenomenon alone cannot be responsible for dry spells over Peninsular Malaysia, as quite a number of equally relatively dry years have been recorded during the absence of the El Niño. However, most La Nina events have resulted in wet years for Peninsular Malaysia with the exception of 1998 and 1955.

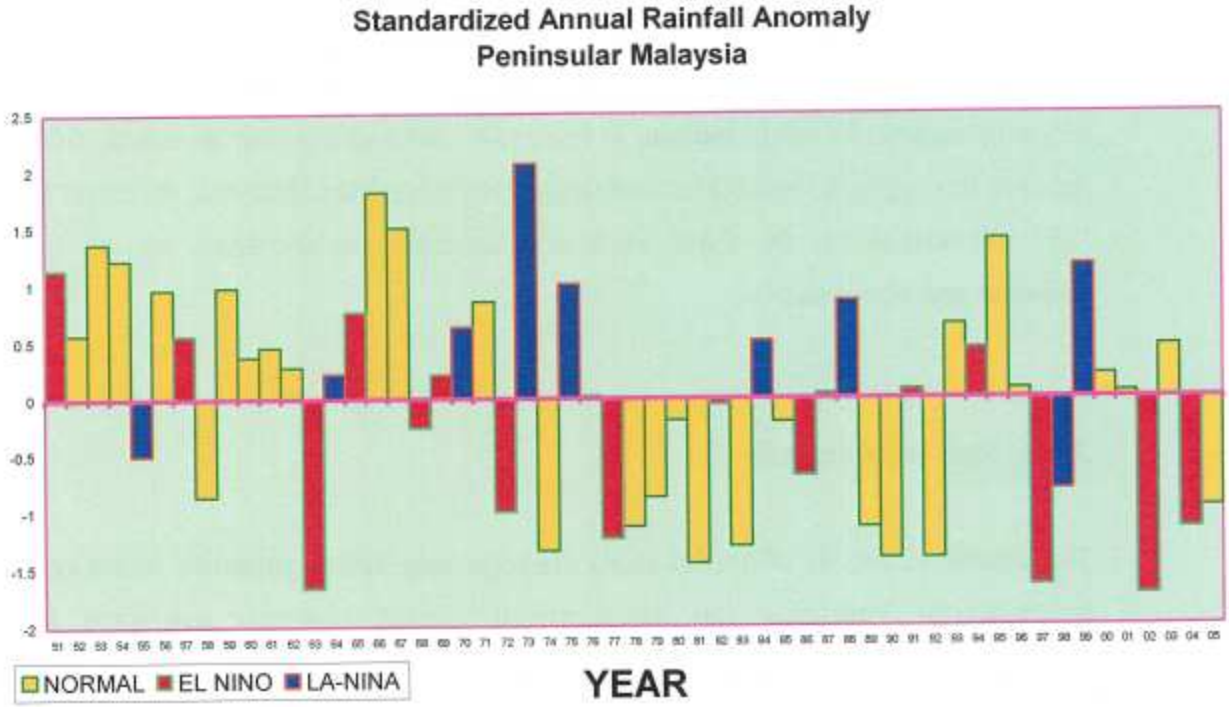

Figure 8: Long Term Standardized Rainfall Anomaly for Peninsular Malaysia

Neither an increasing nor decreasing trend for rainfall was found for East Malaysia during the observed 50 years period (**Figure 9**). Nevertheless the intensity and frequency of the dry years as of 1970 have increased when compared to those of the earlier period. Though the dry years are more frequent than the wet years, the intensity of rainfall increase during the wet years is comparable to those of the decrease in rainfall during the dry years. The La Nina phenomenon is responsible for the three wettest years recorded (1984, 1988 and 1999) for East Malaysia. Most of the relatively severe dry spells in East Malaysia were recorded during the El Niño events except 1978, 1990 and 1992. The El Niño events have greater influence in rainfall reduction in East Malaysia as compared to Peninsular Malaysia.

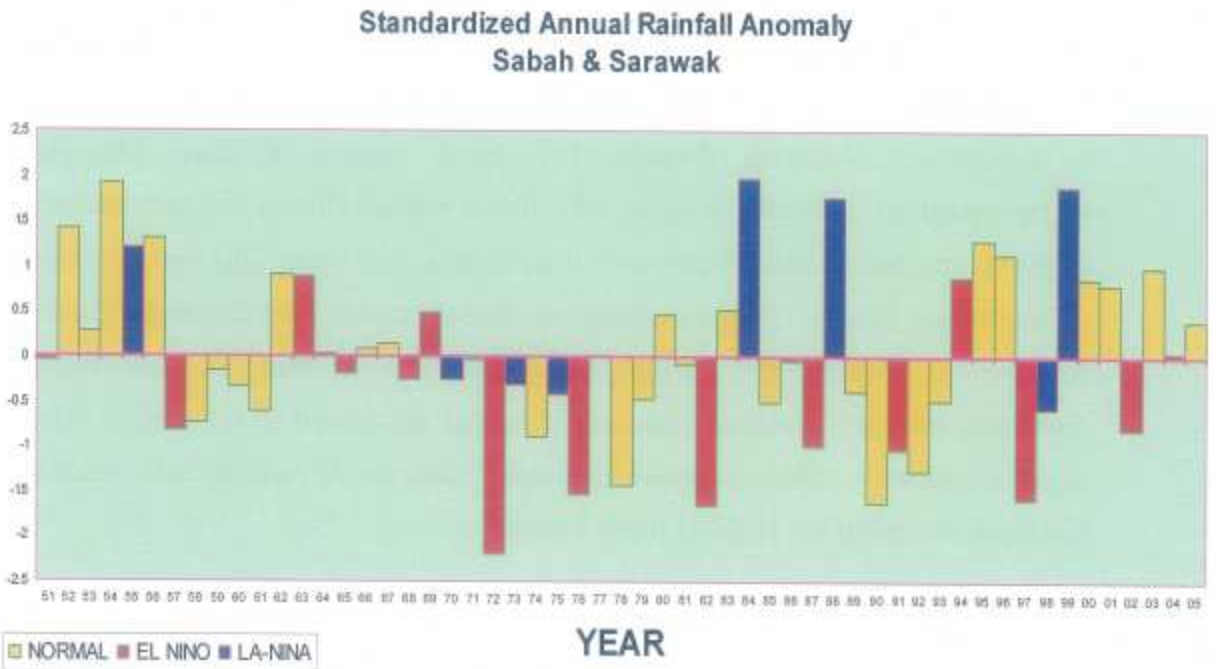

Figure 9: Long Term Standardized Rainfall Anomaly for East Malaysia

Figures 10 and **11** also show the variation in seasonal precipiation patterns for Peninsular Malaysia and East Malaysia respectively. As shown in **Figure 10** a decreasing seasonal rainfall trend for Peninsular Malaysia in 1998-2007 can be observed as compared to those in 1961-1990, except for JJA. Among the seasons, JJA and MAM are the wettest and driest seasons respectively for Peninsular Malaysia. Difference in seasonal rainfall patterns between the western peninsular Malaysia and eastern peninsular Malaysia is most evident in SON and DJF. In SON, eastern Peninsular Malaysia experiences higher rainfall than western Peninsular Malaysia. Though not as obvious as in SON, western Peninsular Malaysia experiences higher rainfall than eastern Peninsular Malaysia in DJF. North western Peninsular Malaysia generally experiences minimal seasonal rainfall during SON as compared to other regions.

Comparing the seasonal rainfall trend in 1961-1990 with those in 1998-2007, East Malaysia shows an increasing trend as opposed to the decreasing trend in Peninsular Malaysia (**Figure 11**). Most regions in East Malaysia experienced an increase of up to 100 mm in rainfall during the two periods. Highest increase in rainfall between the periods was up to 200 mm recorded in south-east Sabah. Sabah experiences lesser rainfall than Sarawak. Sabah experiences minimum and maximum rainfall during DJF and JJA respectively. Generally northern Sarawak has lesser rainfall compared to the rest of other regions except in MAM. Sarawak has maximum rainfall in SON with western Sarawak receiving the highest rainfall amount.

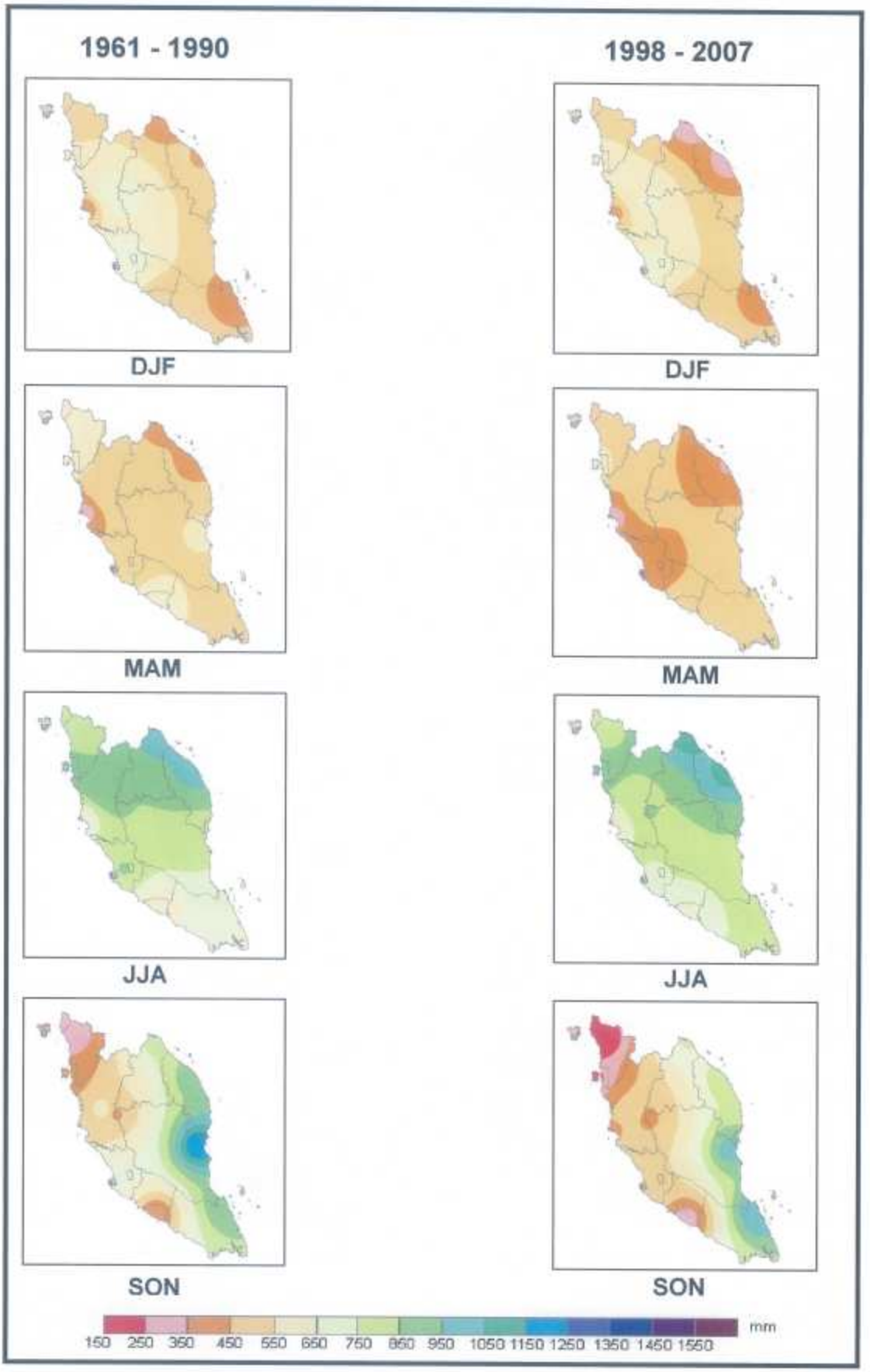

Figure 10: Long Term Mean Rainfall for Peninsular Malaysia

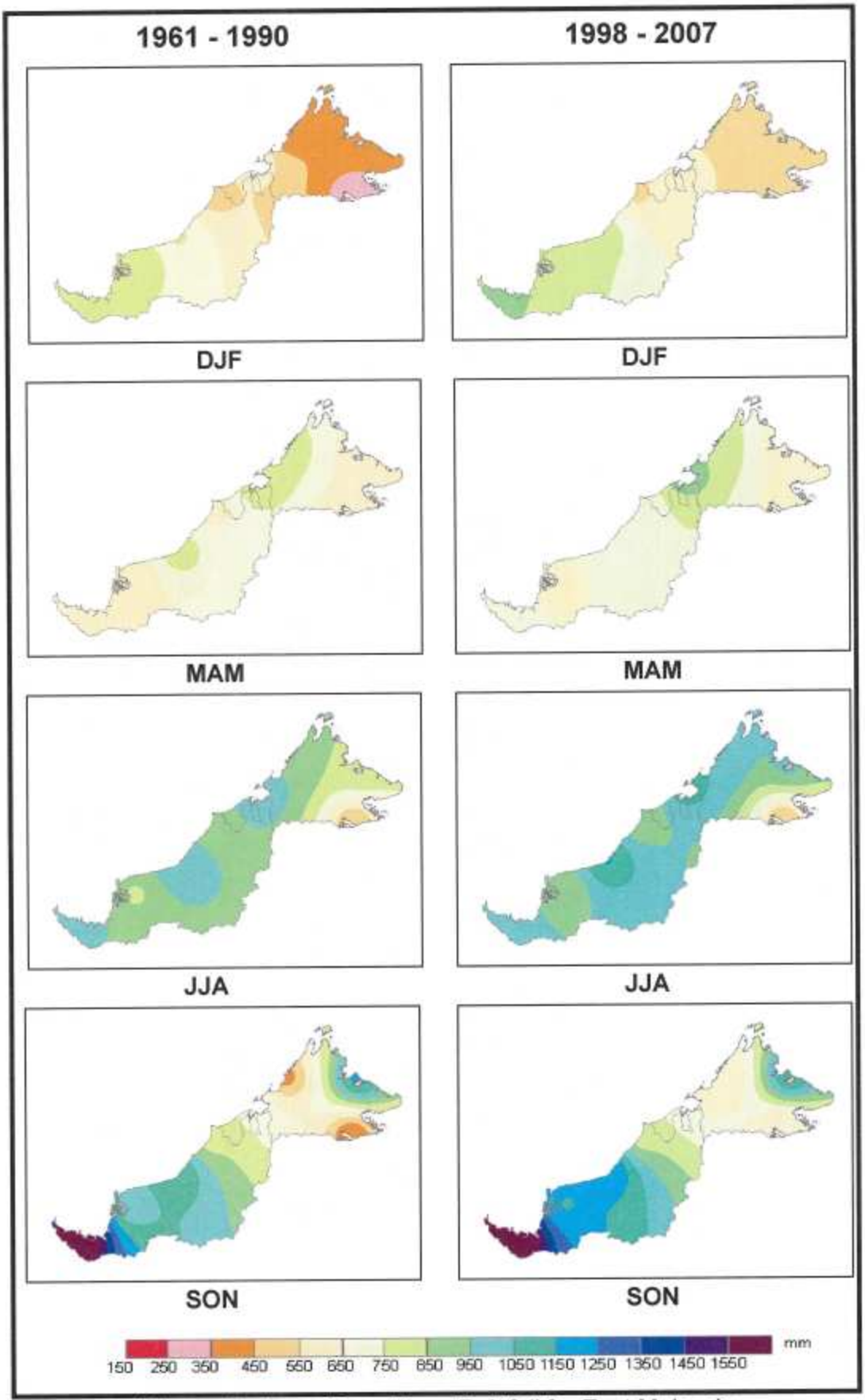

Figure 11: Long Term Mean Rainfall for East Malaysia

Chapter 3: Global General Circulation Models (GCM) - Simulation on the Asian Winter Monsoon

The past and current observed data and models projection of future climates show a picture of a warming future climate along with other variability and extremes. The world is very concerned of the frequency and magnitude of extreme events in the future. In the recent years the occurrence of extreme weather events in Malaysia has increased. The winter monsoon of 2006/2007 and 2007/2008 brought in heavy rainfall and caused severe floods in Malaysia. The heavy rainfall during the winter monsoon of 2006/2007 was the worst ever recorded over southern Peninsular Malaysia. Other extreme events such as flash floods, strong winds and waterspouts have become more frequent over the recent years. The socio-economic impacts of these extreme events have been a cause for concern for the country.

With global warming, extreme weather and climate events including droughts, heavy precipitation, heat waves and severe tropical cyclones have shown significant changes in intensity, areas and frequency of occurrence. According to IPCC's 4^{th} Assessment Report, more intense and longer droughts have been observed over wider areas since the 1970's. The frequency of heavy precipitation events has increased over most land areas. Widespread occurrences in extreme temperature have been observed over the last 50 years. Cold days, cold nights and frost have become less often, while hot day, hot nights, and heat waves have become more frequent. There are observational evidences showing an increase of higher intensity tropical cyclones since the 1970's, correlated with the increase of tropical sea surface temperature. However, there is no clear trend showing an increase in the annual number of tropical cyclones occurrences.

It is very likely that the hot and extreme heat waves and heavy precipitation will continue to become more frequent and future tropical cyclones will become more intense, with higher peak wind speeds and heavier precipitation associated with ongoing increases of tropical sea surface temperature (SST).

Areas affected by droughts will likely increase and the incidence of extreme high sea level will also increase.

3.1 Climate Change Scenario from Nine AOGCMs

The impact of global warming on the monsoons over the Malaysian region is studied by using twelve coupled Atmosphere-Ocean General Circulation Models (AOGCMs). However, for temperature and rainfall analysis, only nine different AOGCMs were chosen in this study. The AOGCMs used in this study are from the contribution of the Coupled Model Inter-comparison Project (CMIP) to the IPCC 4th Assessment Report. Names, providing institutions, general references and resolution of the twelve AOGCMs used are shown in **Table 1**.

TABLE 1: Name, Institution, General Reference and Resolution of AOGCM Models

Model	Institution	Resolution
CNCM3	Meteo-France	2.8° x 2.8°
MRCGCM	Meteorological Research Institute, Japan	T42 (≈2.8°x 2.8°)
FGOALS	Institute of Atmospheric Physics, China	T42 (≈2.8°x 2.8°)
GFCM20	NOAA/GFDL, USA	2.5° x 2.0°
HADCM3	Hadley Centre, UK	3.75°x 2.5°
MIHR	JAMSTEC, Japan	T42 (≈2.8°x 2.8°)
MPEH5	Max Plank Institute, Germany	T63 (≈1.8°x 1.8°)
NCPCM	NCAR, USA	2.8° x 2.8°
CSMK3	CSIRO Atmospheric Research	2.8° x 2.8°
CGMR	Canadian Centre for Climate Modeling & Analysis	T47 (≈3.75°x 3.75°)
MIMR	University Of Tokyo	3.75°x2.5°

All the models start their integration from the '20th Century Climate in Coupled Model' (20C3M) run, in which the level of anthropogenic forcing is based on historical data of the late 19th century through the 20th century. From the end of the 20C3M run, SRES-A1B conditions is imposed and integrated till the year 2100.

The model control period is selected as the average of 1990–1999 of the 20C3M run and compared against the SRES-A1B scenario for the period 2020 – 2029, 2050 – 2059 and 2090 - 2099. The parameters analysed were the changes in precipitation and temperature over the region 90°E – 130°E, 5°S – 15°N. In addition to the above analysis, a 5-year running mean was used to show the change in precipitation in comparison to the baseline period of 1961-1990 for Peninsular Malaysia, Sarawak and Sabah for the SRES A1B scenario (areas selected for this study are as shown in **Figure 12**). An ensemble projection for temperature and precipitation of the nine AOGCMs were plotted for the period 2000 – 2100 for the SRES A1B scenario.

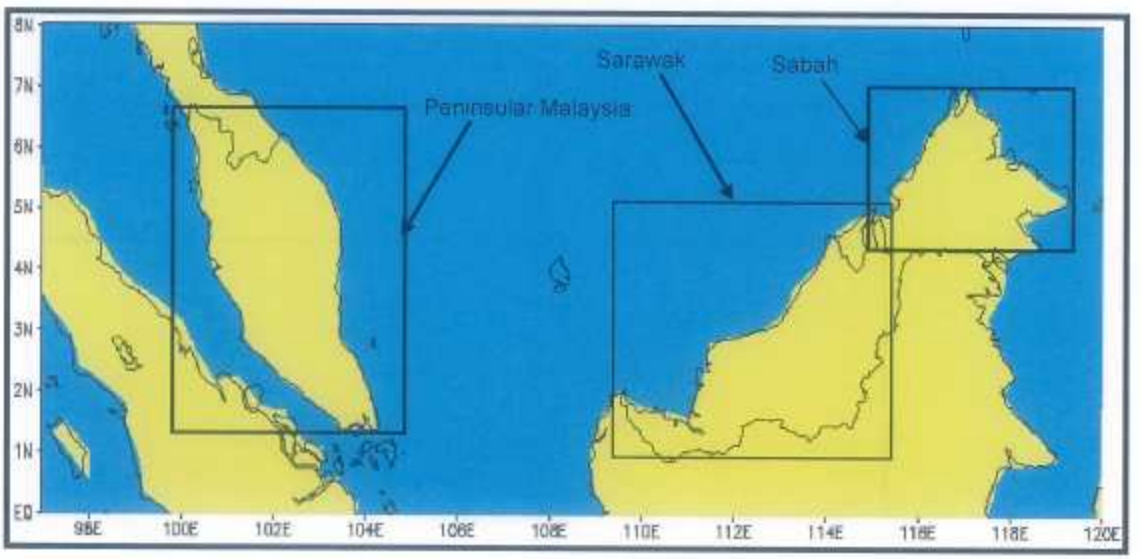

FIGURE 12: Selected domains over the Malaysian region.

3.1.1 Temperature Trends

Outputs generated by the AOGCMs show that all the models projected an increase in temperature for Peninsular Malaysia (**Figure 13**), Sabah (**Figure 14**) and Sarawak (**Figure 15**) but the degree of temperature increase varies from model to model. The range of temperature increase at the end of the 21st century over the 3 domains is as shown in the respective figures. An ensemble mean of the entire nine AOGCM models indicate an increasing temperature trend for the 3 domains, Peninsular Malaysia (**Figure 16**), Sabah (**Figure 17**) and Sarawak (**Figure 18**).

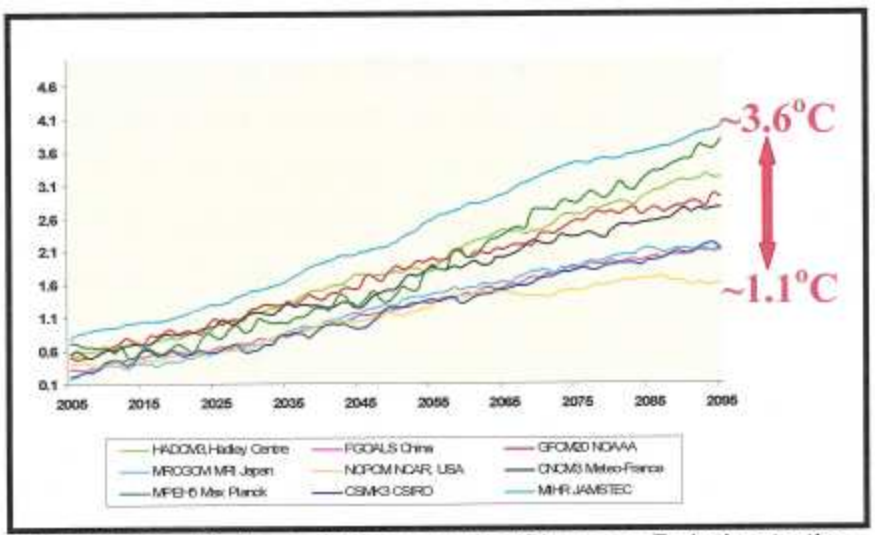

FIGURE 13: Projected Temperature Changes Relative to the Baseline (1961-1990) for Peninsular Malaysia from Nine GCMs, Based on SRES A1B

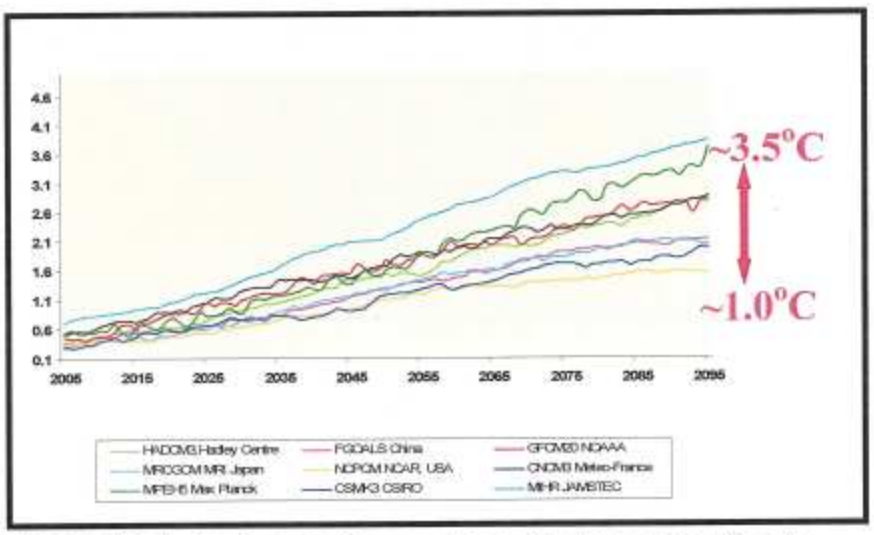

FIGURE 14: Projected Temperature Changes Relative to the Baseline (1961-1990) for Sabah from Nine GCMs, Based on SRES A1B

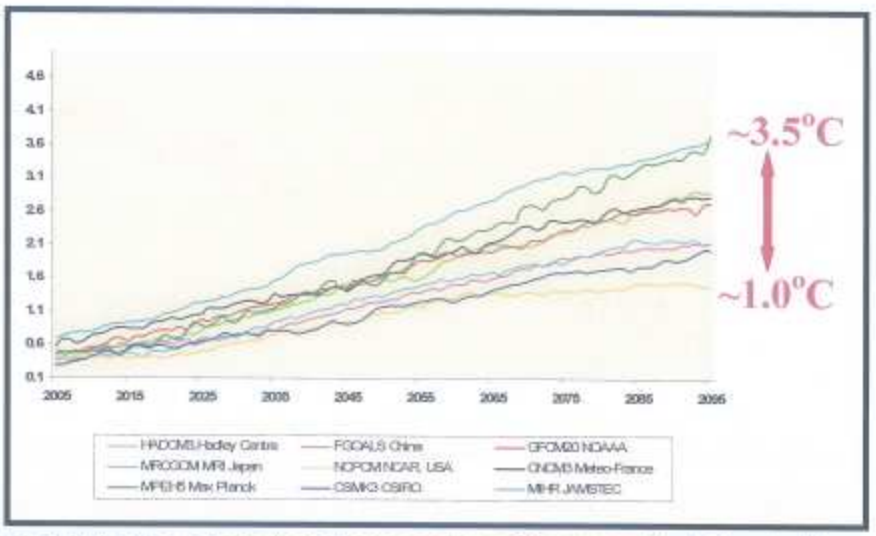

FIGURE 15: Projected Temperature Changes Relative to the Baseline (1961-1990) for Sarawak from Nine GCMs, Based on SRES A1B

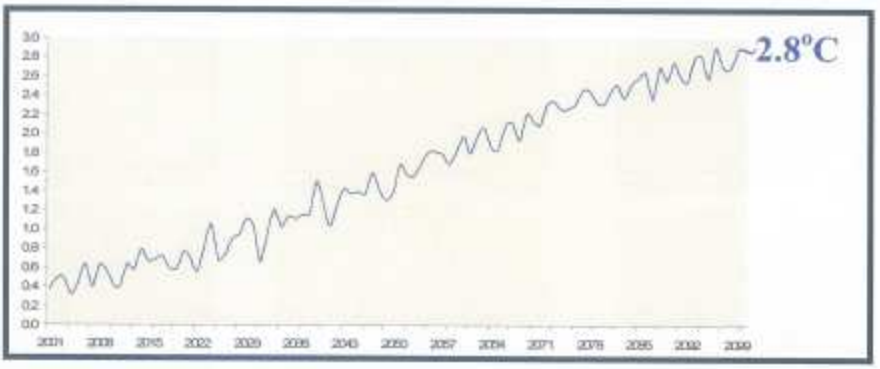

FIGURE 16: Ensemble Mean Projected Temperature Changes Relative to the Baseline (1961-1990) for Peninsular Malaysia from Nine GCMs, Based on SRES A1B

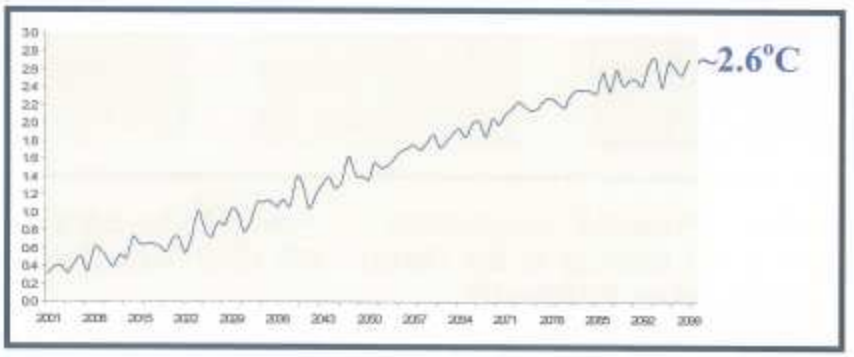

FIGURE 17: Ensemble Mean Projected Temperature Changes Relative to the Baseline (1961-1990) for Sabah from Nine GCMs, Based on SRES A1B

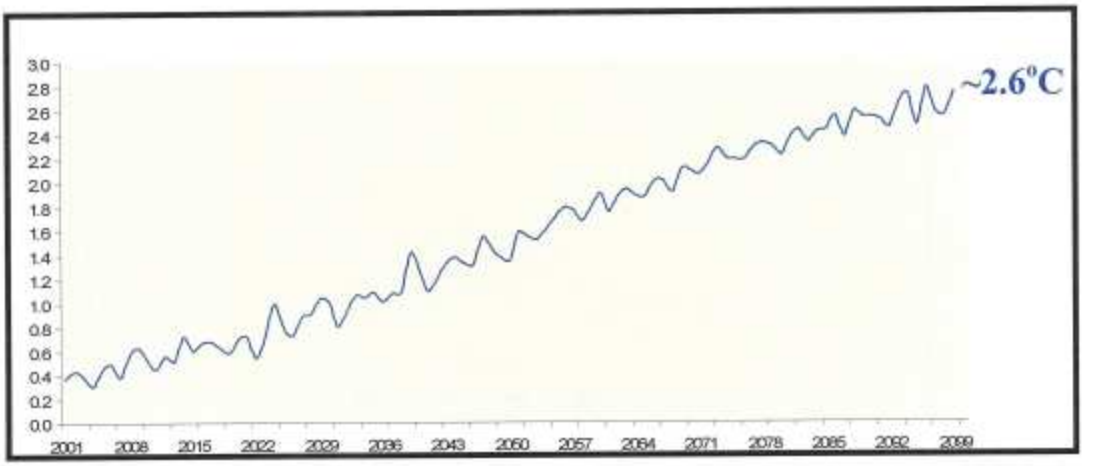

FIGURE 18: Ensemble Mean Projected Temperature Changes Relative to the Baseline (1961-1990) for Sarawak from Nine GCMs, Based on SRES A1B

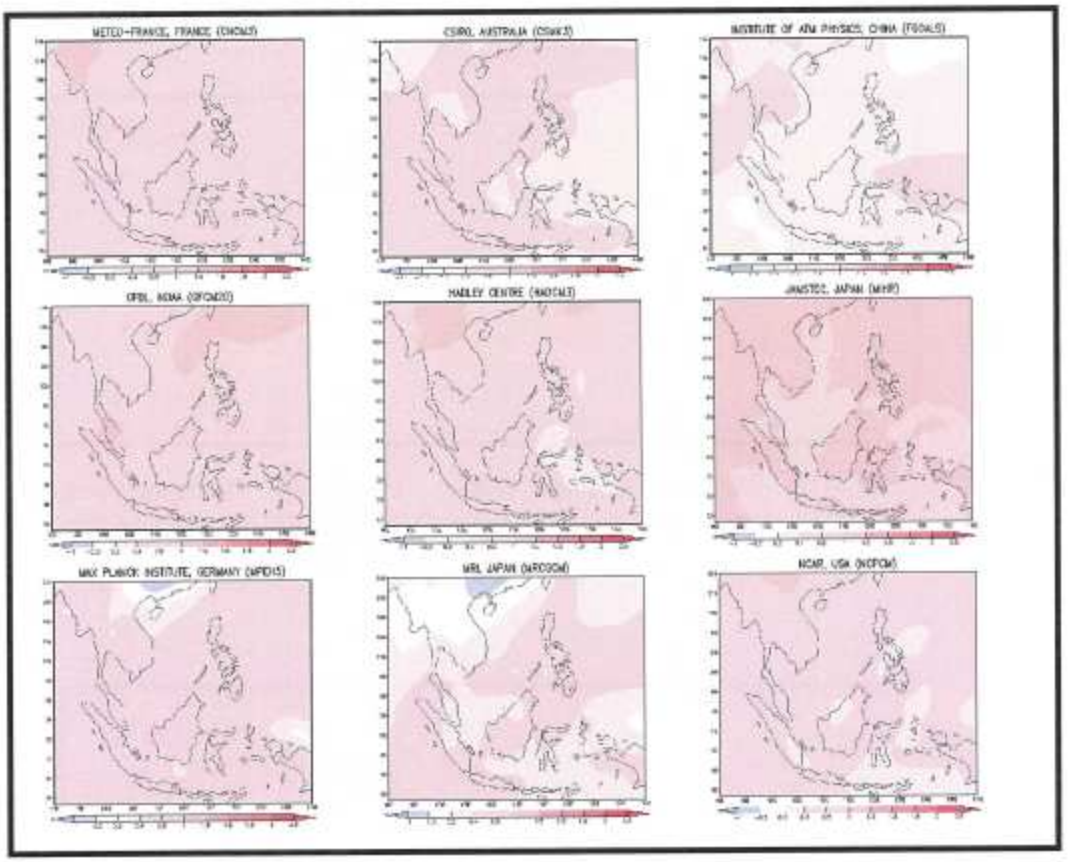

FIGURE 19: Projected Temperature Changes (°C) for Early of 21st Century (2020 – 2029) Relative to the Period 1990-1999 (Last Decade of the 20th Century) Based on SRES A1B

FIGURE 20: Projected Temperature Changes (˚C) for Middle of 21st Century (2050 – 2059) Relative to the Period 1990-1999 (Last Decade of the 20th Century) Based on SRES A1B

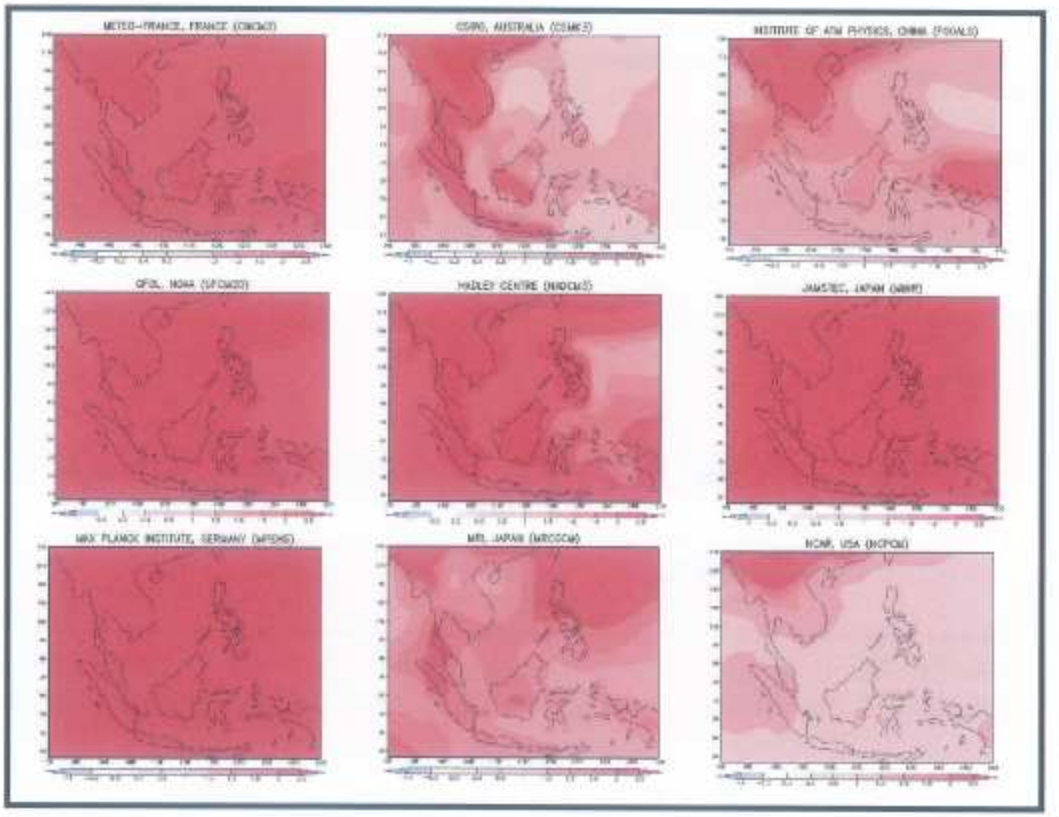

FIGURE 21: Projected Temperature Changes (˚C) for the late 21st Century (2090 – 2099) Relative to the Period 1990-1999 (Last Decade of the 20th Century) Based on SRES A1B

Further analysis shows that the increase in temperature is most apparent towards the late 21st century (2090 – 2099). Projected Temperature Changes for the early 21st century, middle of 21st century and the late 21st Century (2090 – 2099) relative to the Period 1990-1999 (last decade of the 20th century) based on SRES A1B are as shown in **Figures 19**, **20** and **21** respectively.

3.1.2 Rainfall Trends

As for the change in rainfall, there is no clear trend shown by all of the selected models due to the high variability in the precipitation-modulating factor. The 10-year running mean precipitation projections for Peninsular Malaysia, Sabah and Sarawak are as shown in **Figures 22**, **23** and **24** respectively.

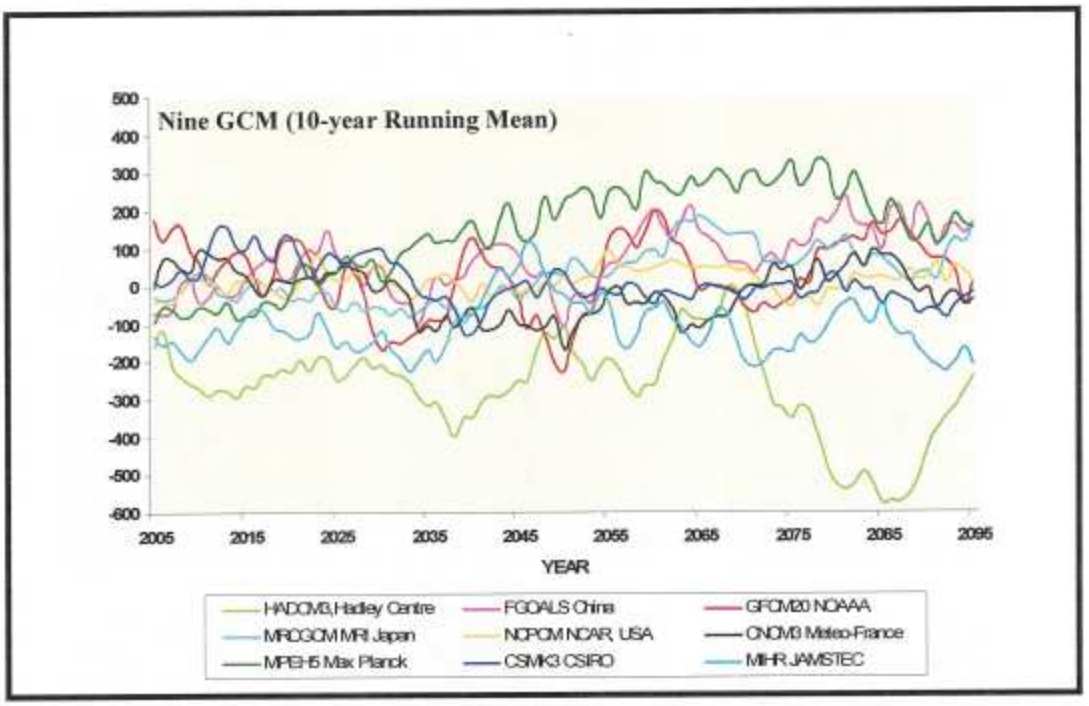

FIGURE 22: Projected Rainfall Changes (mm) Relative to the Baseline (1961-1990) for Peninsular Malaysia from Nine GCMs, Based on SRES

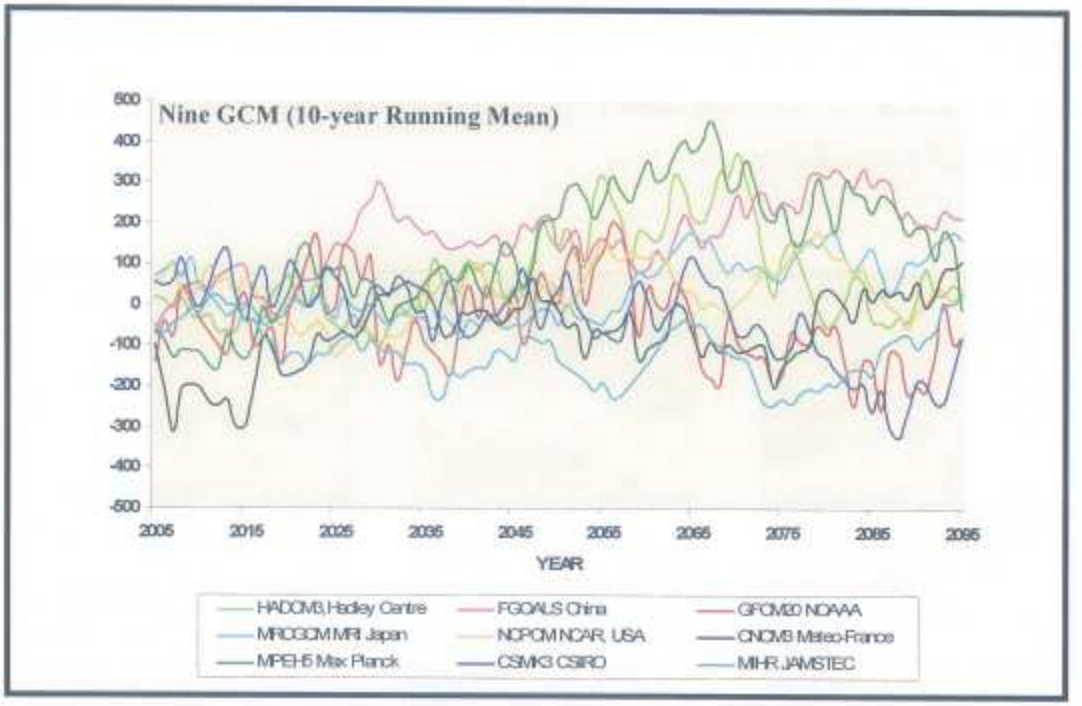

FIGURE 23: Projected Rainfall Changes (mm) Relative to the Baseline (1961-1990) for Sabah from Nine GCMs, Based on SRES A1B

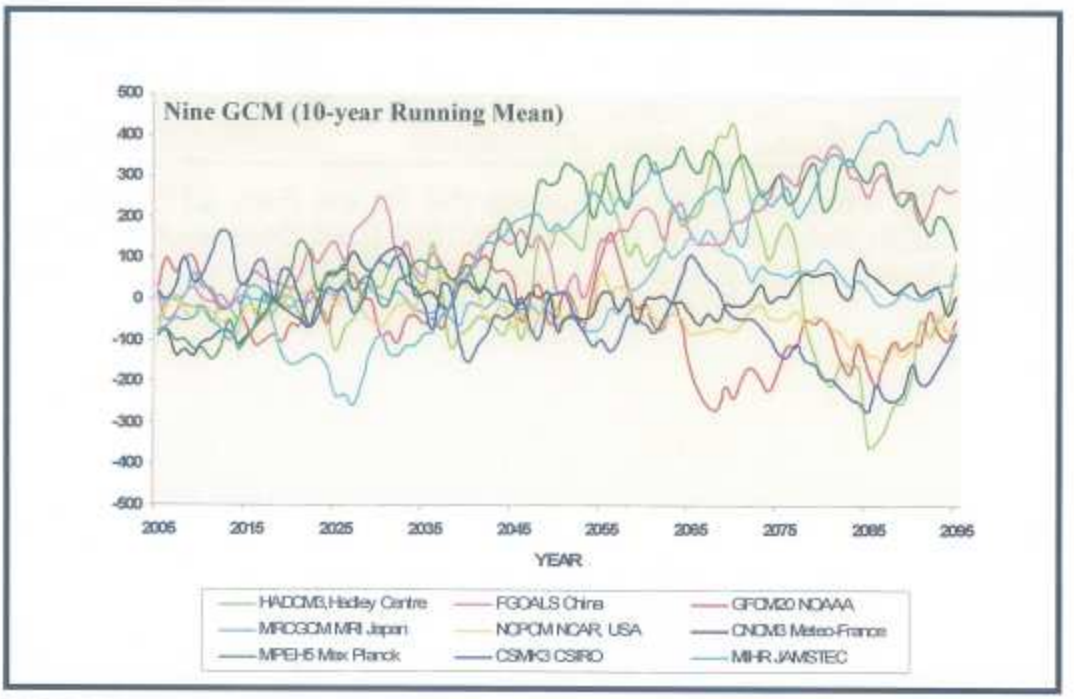

FIGURE 24: Projected Rainfall Changes (mm) Relative to the Baseline (1961-1990) for Sarawak from Nine GCMs, Based on SRES A1B

Projected rainfall changes for the early 21st century, middle of 21st century and the late 21st Century (2090 – 2099) relative to the Period 1990-1999 (last decade of the 20th century) based on SRES A1B are as shown in **Figures 25**, **26** and **27** respectively.

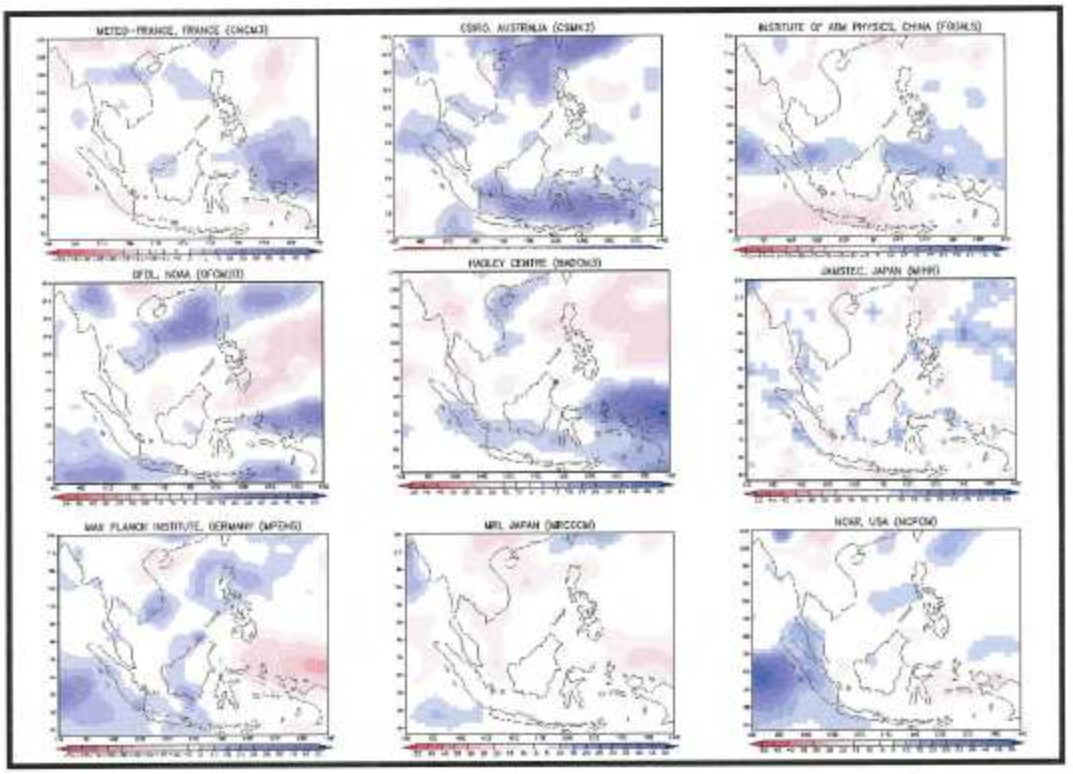

FIGURE 25: Projected Rainfall Changes (%) for the Early 21st Century (2020 – 2029) Relative to the Period 1990-1999 (Last Decade of the 20th Century) Based on SRES A1B

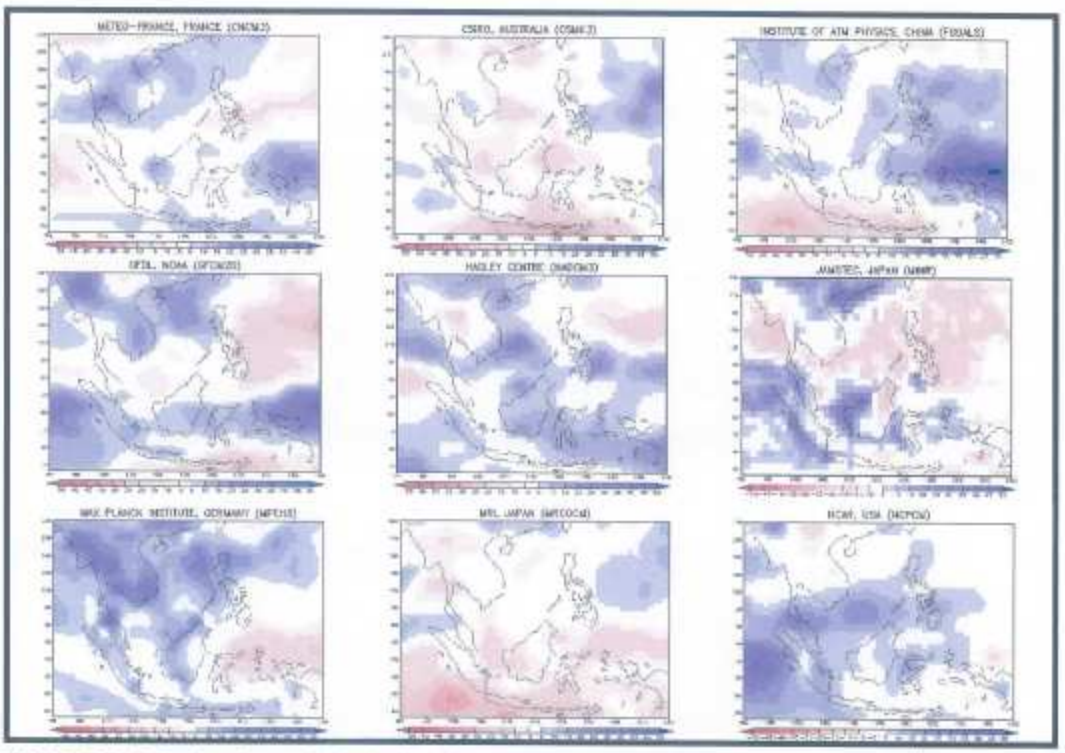

FIGURE 26: Projected Rainfall Changes (%) for the Middle of 21st Century (2050 – 2059) Relative to the Period 1990-1999 (Last Decade of the 20th Century) Based on SRES A1B

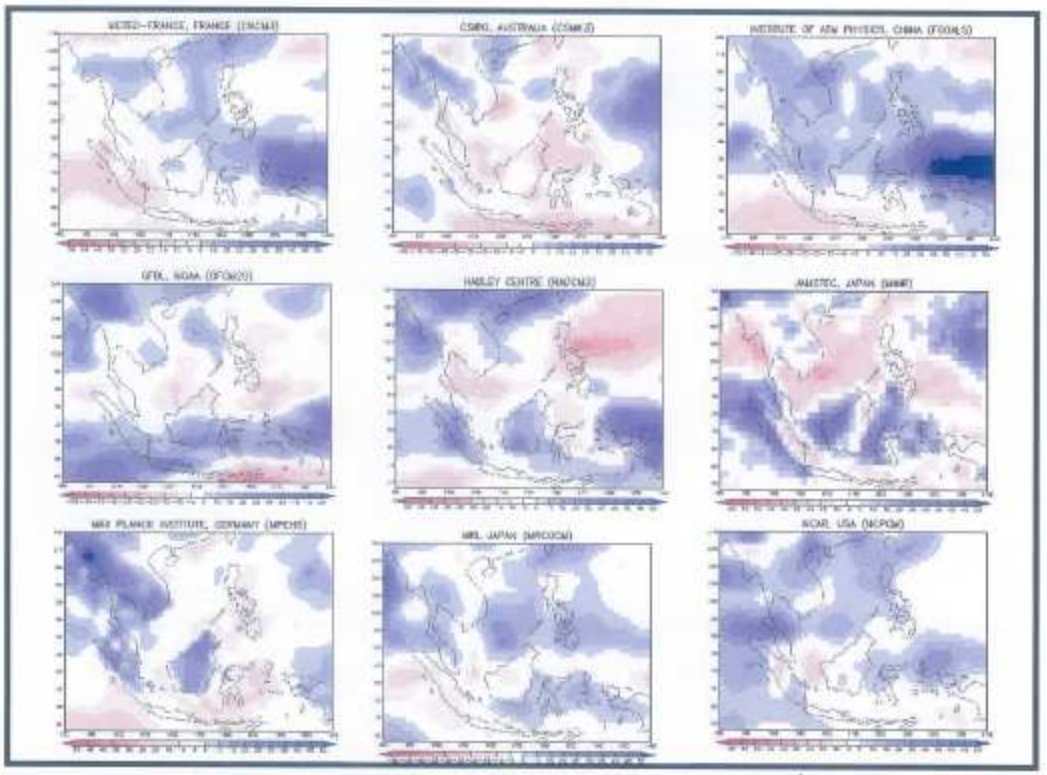

FIGURE 27: Projected Rainfall Changes (%) for Late 21st Century (2090 – 2099) Relative to the Period 1990-1999 (Last Decade of the 20th Century) Based on SRES A1B

3.1.3 Ensemble Rainfall Projection

Based on the MMD's surface observation stations data, annual rainfall change (percentage) for the periods 2000 - 2007 relative to the period 1990 - 1999 (Last Decade of the 20th Century) as shown in **Figure 28(a)**, indicate that west coast of Peninsular Malaysia has an increase of 6 - 10 % in rainfall amount, whereas a decrease of 4 – 6 of rainfall amount over central Pahang and coastal Kelantan. As for East Malaysia, Sarawak has an increase of 6 – 10 % in rainfall amount and Sabah has an increase of more than 10%.

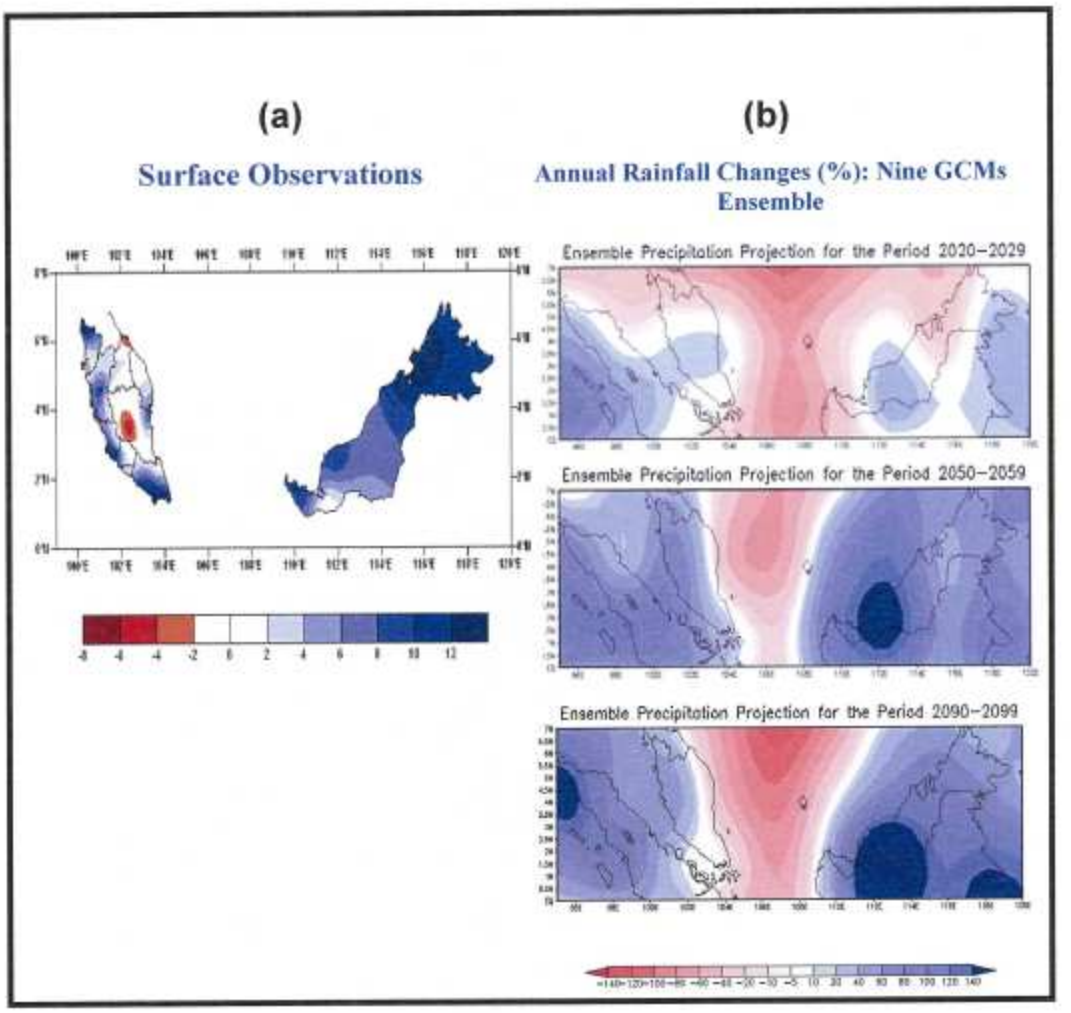

FIGURE 28: Comparison of Annual Rainfall Change (%): (a) For The Period 2000 – 2007 Relative To The Period 1990-1999 (Last Decade of the 20th Century), based on the MMD's Surface Observation Stations Data; and (b) for The Periods 2020–2029, 2050–2059, and 2090–2099 Relative To The Period 1990-1999 based on the Nine AOGCM Ensemble.

The ensemble rainfall projection for the nine AOGCM for the 21st century exhibit an increase in precipitation over the West Coast states and a decrease over the East Coast states of Peninsular Malaysia (**Figure 28(b)**). For East Malaysia, the AOGCM models have projected the rainfall over western Sarawak to increase significantly by the end of the 21st century.

3.2 The Winter Monsoon Circulation

Winter Monsoon (DJF) averaged 850hPa wind for the nine selected AOGCMs climatology (1961-1990) (**Figure 29**) and the ensemble of the nine AOGCM climatology (1961-1990) (**Figure 30**) depict the general circulation pattern during the winter monsoon period (DJF). The strong northeasterly winds are a prominent feature over the South China Sea region.

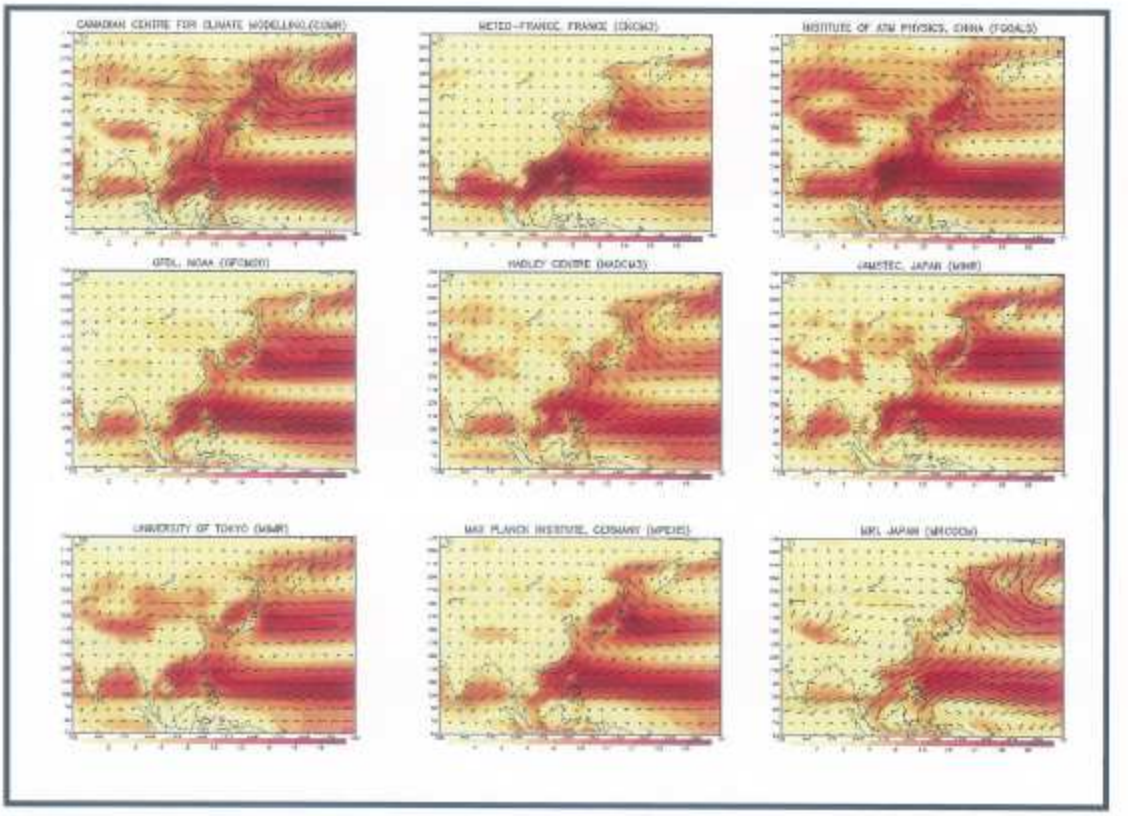

FIGURE 29: Winter Monsoon (DJF) Averaged 850 hPa Wind (m/s) for the Nine Selected AOGCMs (1961-1990)

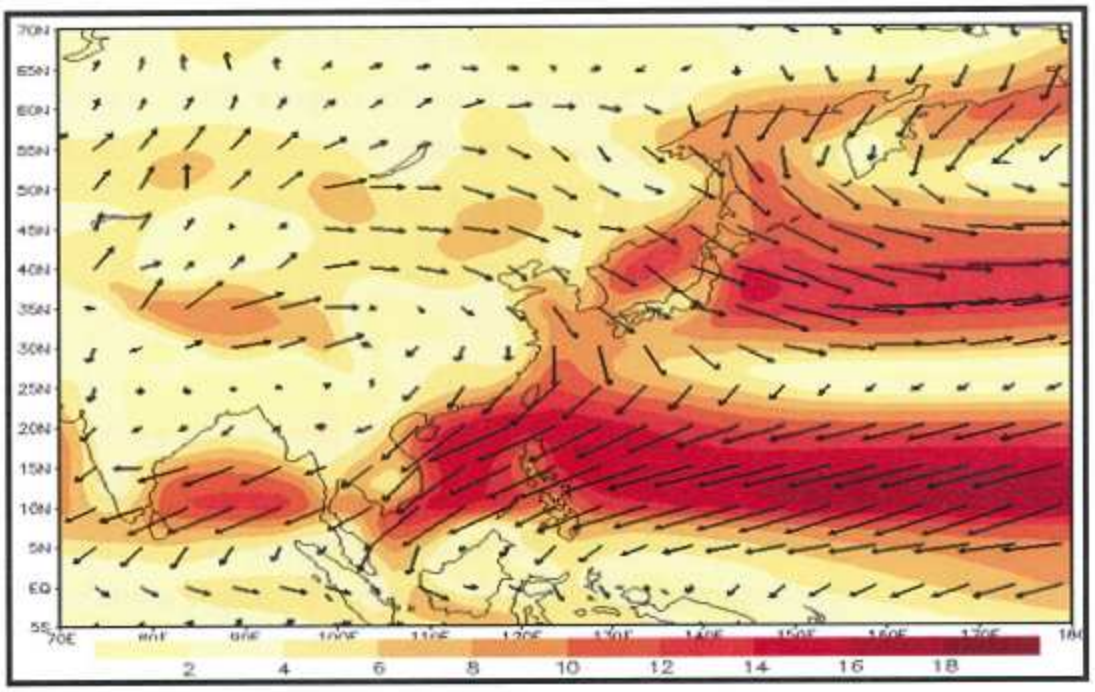

FIGURE 30: Winter Monsoon (DJF) Averaged 850hPa Wind (m/s) for the AOGCM Models Ensemble Climatology (1961-1990)

3.3 The Winter Monsoon Intensity

The Winter Monsoon Intensity Index defined by Zhou *et. al* is used to gauge the intensity or severity of the Northeast Monsoon (Winter Monsoon). This index is also used to analyse the interannual variability of the Asian monsoon, particularly the Northeast monsoon. Winter Monsoon Index (WMI) is defined as the area averaged SLP (sea level pressure) anomaly difference between (**110-120°E, 20-45°N**) and (**150-160°E, 20-45°N**).

The marked features for a strong (weak) winter monsoon include strong (weak) northerly winds along coastal East Asia, cold (warm) East Asian continent and surrounding sea and warm (cold) ocean from the subtropical central Pacific to the tropical western Pacific, high (low) pressure in East Asian continent and low (high) pressure in the adjacent ocean and deep (weak) East Asian trough at 500hPa level.

The interannual variations are found to be closely connected to the sea surface temperature (SST) anomaly in both the western and eastern tropical Pacific. The results suggest that the processes associated with the SST anomaly over the tropical Pacific mainly influence the strength of the winter monsoon. The winter monsoon generally becomes weak when there is a positive SST anomaly in the tropical eastern Pacific (El Niño), and it becomes strong when there is a negative SST anomaly (La Niña). Moreover, the SST anomaly in the South China Sea is found to be closely related to the winter monsoon and may persist to the following summer.

During the winter monsoon, the maritime continent experiences increased convective activity due to the strengthening of the East Asia branch of the north-south Hadley circulation and the east-west Walker circulation. This is primarily due to extensive freshening of the low-level northeasterlies associated with a cold surge, which penetrates rapidly into the equatorial South China Sea enhancing the low-level convergence in the near-equatorial region. The impact on the low-level convergence depends on the degree of the air-sea interaction caused by the northeasterly surge. The warm equatorial waters interact with the colder waters in the South China Sea creating a temperature gradient perpendicular to the Borneo coast. The sea surface temperature (SST) gradient over the South China Sea extending from 3°N to 9°N and 104°E to 116°E are mainly driven by the easterly and northeasterly winds. The SST gradient enhances the near-equatorial vortices by intensifying the convective activities in the near-equatorial regions of the South China Sea. The 850hPa vorticity and the averaged SST gradient are used to show the interaction between the South China Sea SST and the near-equatorial vortices.

3.4 Winter Monsoon Projections

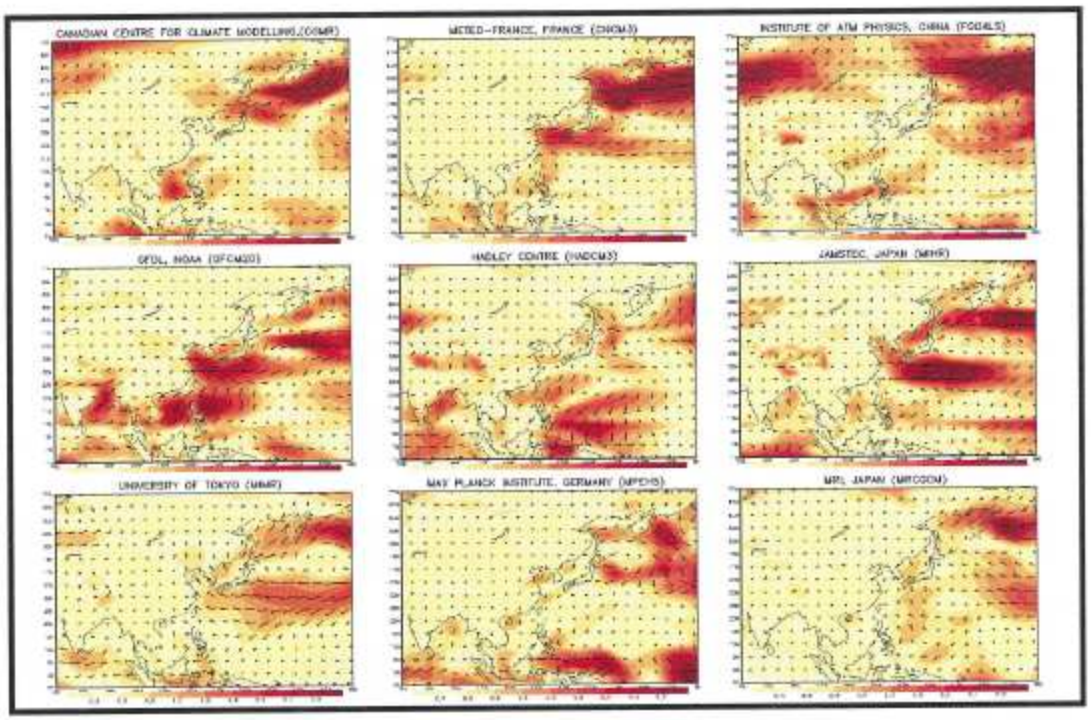

FIGURE 31: Projected Wind Anomaly for the Winter Monsoon Season (DJF) During the Early 21st Century (2020-2029) Relative to the Period 1990-1999 (Last Decade of the 20th Century) Based on SRES A1B

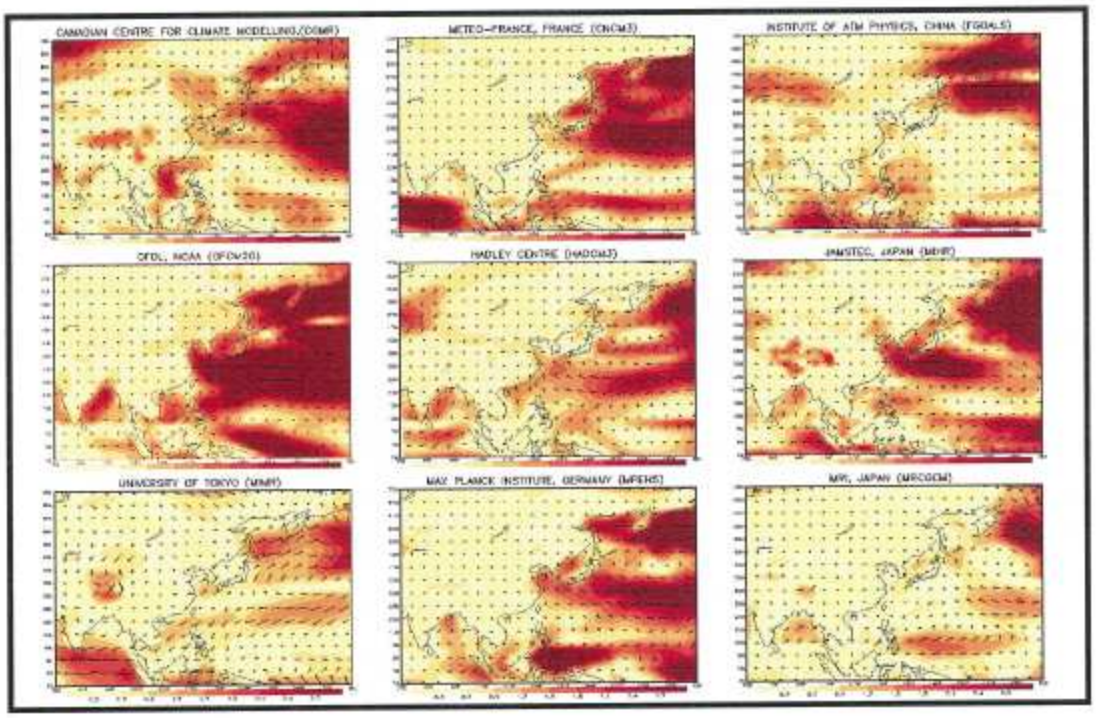

FIGURE 32: Projected Wind Anomaly for the Winter Monsoon Season (DJF) During the Late 21st Century (2090-2099) Relative to the Period 1990-1999 (Last Decade of the 20th Century) Based on SRES A1B

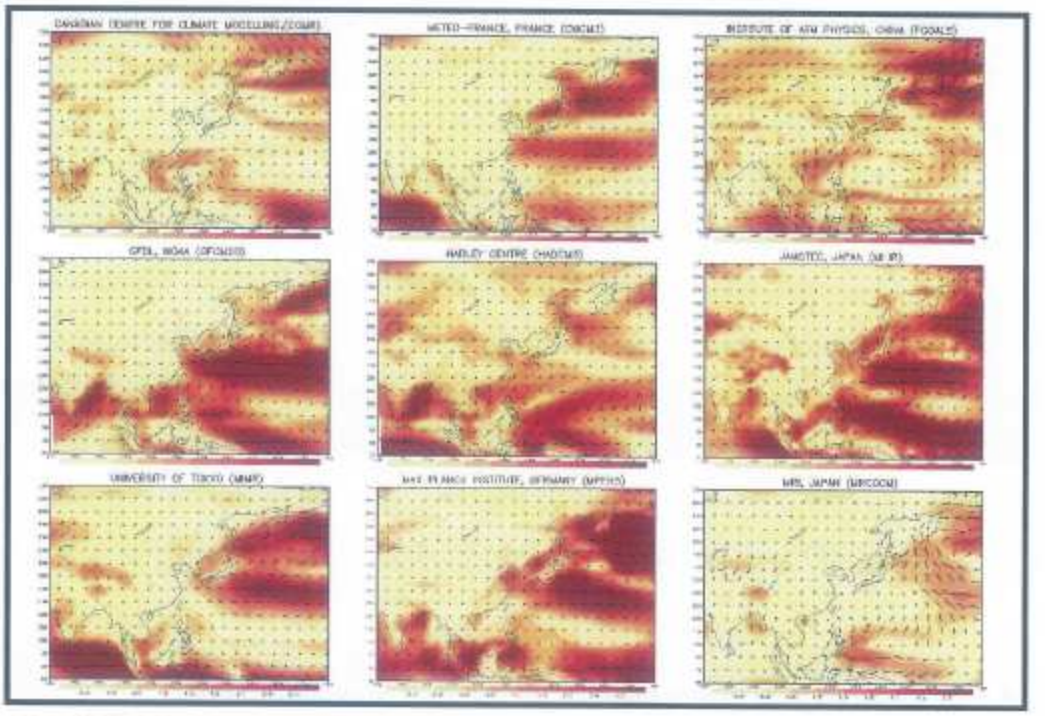

FIGURE 33: Projected Wind Anomaly for the Winter Monsoon Season (DJF) During the Late 21st Century (2090-2099) Relative to the Period 1990-1999 (Last Decade of the 20th Century) Based on SRES A1B

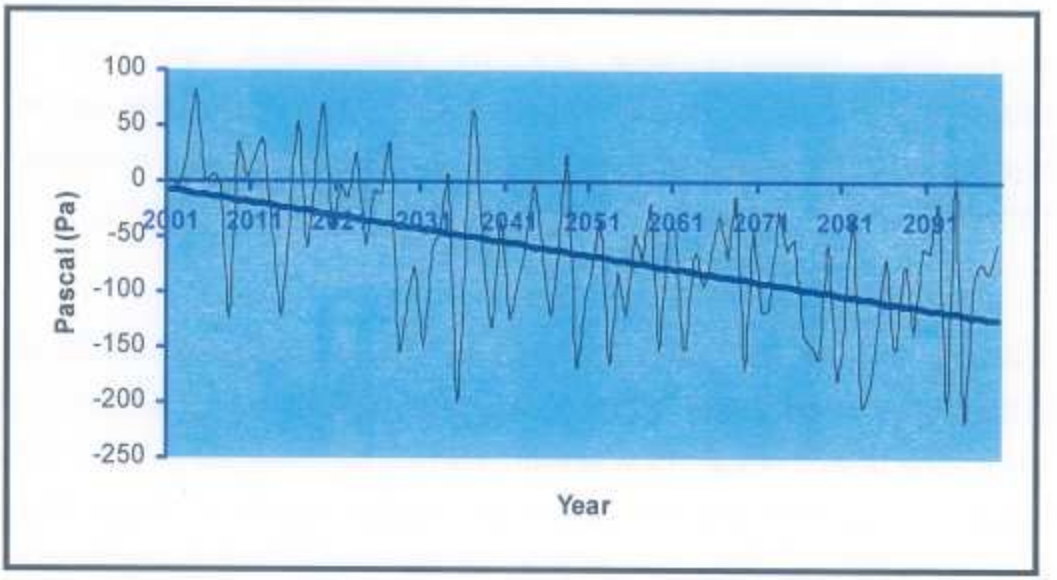

FIGURE 34: Nine AOGCM Ensemble Projection of the Winter Monsoon Index

The projected 850hPa wind anomaly for the winter monsoon season (DJF) during the early 21st century (2020-2029) (**Figure 31**), middle of 21st century (2050 – 2059) (**Figure 32**) and the late 21st century (2090-2099) (**Figure 33**) relative to the period 1990-1999 (last decade of the 20th century) based on SRES A1B scenario indicate the slackening of the winter monsoon northwesterlies flow over northern China to the Pacific Ocean, the weakening of Siberia High, the weakening and northward shift of the Aleutian Low as well as the apparent weakened pressure gradient in the eastern coast of the Asian continent. The projected 850hPa wind circulation pattern anomaly and the negative trends in the ensemble projection of the Winter Monsoon Index (2001 – 2099) (**Figure 34**) show the overall weakening of the winter monsoon.

3.5 The Northeast Monsoon of 2006/2007 and 2007/2008

The northeast monsoon of 2006/2007 and 2007/2008 brought a lot of rainfall and floods to Malaysia and Indonesia. The rainfall during the northeast monsoon of 2006/2007 was the worst ever recorded over southern Peninsular Malaysia. The 2007/2008 northeast monsoon, however, brought heavy rainfall over different localized areas. By examining the sea surface temperature (SST) data, reanalysis data and the observational data from the meteorological stations, we can determine the major synoptic features which contributed to the heavy rainfall episodes during the northeast monsoon of 2006/2007 and 2007/2008 over Malaysia.

The winter of 2006/2007 was a warm winter. Some of the main characteristics of the winter of 2006/2007 were the late onset of the northeast monsoon, the late ending of the tropical storm season, warmer SST over the western Indian Ocean, warmer SST over the central and eastern equatorial Pacific Ocean due to El Niño and also the late onset of the Australia/Indonesia monsoon trough. During the northeast monsoon of 2006/2007, eastward-propagating Madden-Julian Oscillation (MJO) disturbance caused heavy rainfall in Indonesia and Sarawak between end of December 2006 and early January 2007. However, the abnormally heavy rainfall in mid-December 2006 and mid-

January 2007 that hit southern Peninsular Malaysia was due to strong north-easterly surge with strong cyclonic shear and associated mesoscale cloud systems. The subtropical high over south China had induced strong surges to southern Peninsular Malaysia. These heavy rainfall episodes were not directly related to the MJO disturbance.

The northeast monsoon of 2007/2008 was characterized by positive temperature anomalies over Siberia and mainland China, indicating warmer winter. The cold surges from Siberia and northern China during early part of the northeast monsoon were not intense. The SST anomaly over the central and eastern equatorial Pacific Ocean was negative, indicating a moderate La Niña condition. The northeast monsoon of 2007/2008, which caused heavy precipitations over Malaysia, was directly influenced by the wet phase of MJO between early to mid-December 2007. This caused long and widespread floods over southern Thailand and Malaysia.

Chapter 4: Regional Climate Simulation

Global Circulation Models (GCM) lack the regional detail that impact assessment on climate change required. A Regional Climate Model (RCM) adds small-scale detailed information of future climate change to the large-scale projections of a GCM. They use coarse resolution information from a GCM and then develop temporally and spatially fine scale information. Generally oceans are not modelled in RCMs as this will result in increase of costing and yet will make little difference to projections over land that most impact assessment reports require. Nevertheless the ocean component is already modelled and coupled with the GCM as an Ocean Atmospheric Coupled Global Circulation Model (AOGCM).

The minimum resolution generally used by a RCM is around 50km. Lateral atmospheric boundary conditions are obtained from GCMs. The main advantage of a RCM is that it can provide high-resolution information on a large physically consistent set of climate variables and therefore better representation of extreme events. This is especially so when the land area terrain is composed of mountains and coastlines on scales 100km or less.

4.1 Regional Simulation Experimental Design

For regional climate modeling simulation, the Providing Regional Climates for Impacts Studies (PRECIS) model developed at the Hadley Centre, United Kingdom Met Office is being used in the Malaysian Meteorological Department. Meteorological lateral boundary conditions (LBC) to run the RCM simulations were obtained from the Hadley Centre HadCM3 atmospheric ocean coupled GCM (AOGCM). The HadCM3 is based on the SRES A1B scenario as mentioned in the previous chapter. The HadCM3 regional simulations were done for the periods from 1960 to 2100. The simulation results for 1961 to 1990 are used as the baseline. Results from 2001 to 2099 generate climate change scenarios of the future climate.

SRES A2 and B2 simulations were also done using the PRECIS RCM. LBC for the A2 and B2 simulations were obtained from atmospheric only GCM (AGCM), the HadAM3P. LBC from the HadCM3 AOGCM and sea surface temperature fields were used to generate the HadAM3P AGCM. The HadAM3P AGCMs for both A2 and B2 were run for the specific period or time-slice from 2070 to 2100.

The HadCM3 AOGCM, HadAM3P AGCM and PRECIS RCM are all hydrostatic primitive-equation atmospheric models employing regular latitude-longitudes grids of resolution 2.5° x 3.75°, 1.25° x 1.25° and 0.44° x 0.44° (approximately 50km) respectively. All the three models have 19 vertical levels described by a hybrid vertical coordinate system. The time steps are 30 minutes for the HadCM3 AOGCM and HadAM3P AGCM. Time steps for the PRECIS RCM are 5 minutes. All three models mentioned above are integrated in spherical polar coordinates, with the coordinate pole shifted in the RCM so that its domain appears as a rectangular equatorial segment of a rotated grid. This is to ensure quasi-uniform resolution over area of interest. The estimated evolution of anthropogenic emissions of sulphur dioxide and other relevant chemicals such as dimethyl sulphide and ozone and their impact on atmospheric composition are simulated within the sulphur cycle model of the HadCM3, the HadAM3P and the PRECIS RCM. Before commencing the RCM climate simulation it is necessary to allow the atmosphere and land surface to adjust or "spin-up" to a mutual equilibrium state. The spin-up period considered is one year since the temperature and moisture in deep soil levels can take many months to reach equilibrium with the LBC though it takes only a few days for the atmosphere in the RCM interior. The RCM domain and orographic distribution are as shown in **Figure 35** below.

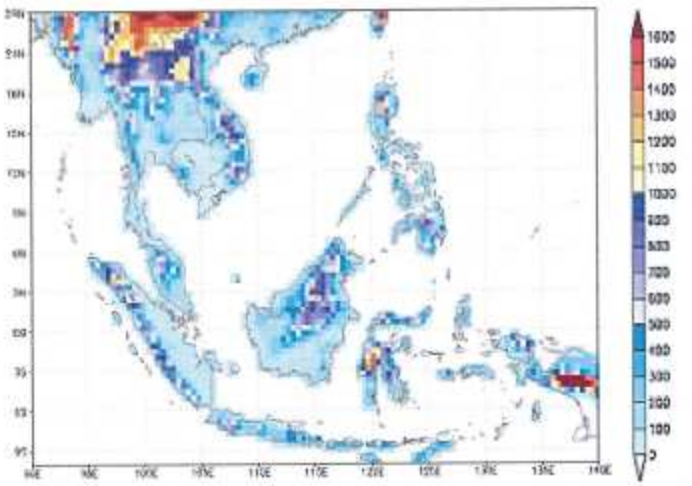

Figure 35: Terrain distribution for Regional Climate Simulation Region

4.2 Validation

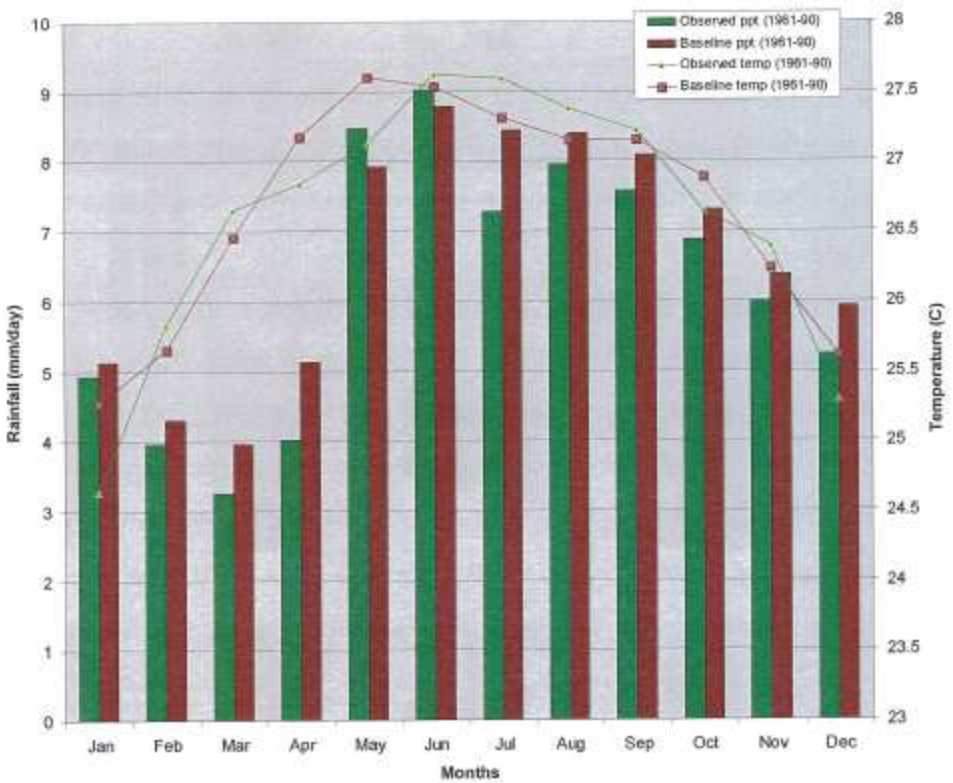

Figure 36: Observed and Baseline Simulation Rainfall and temperature

Comparing the baseline (1961-1990) simulation output with the observed data for the period above, the RCM simulation was validated. Temperature and

rainfall observational data was obtained from the Climate Research Unit of the University of East Anglia, United Kingdom. Resolution of the observed dataset is 60km, which is comparable to regional simulation output of 50km resolution.

Though there is difference in values obtained for both rainfall and temperature between the baseline simulation and the observation, nevertheless the monthly variation trend of the temperature and monthly distribution of rainfall are consistent.

4.3 Changes in Temperature

Seasonal and annual variation trend analyses are used for this report. The definition of the various seasons is as used in the previous chapters. Five-year running means have been used to display trend patterns. The trend patterns have been obtained separately for Peninsular Malaysia, Sabah and Sarawak given that these regions might show different responses to the different climate scenarios used. Temperature and rainfall anomalies were obtained by comparing future decadal simulations with the simulation for the last decade of the 20th century (1990 to 1999).

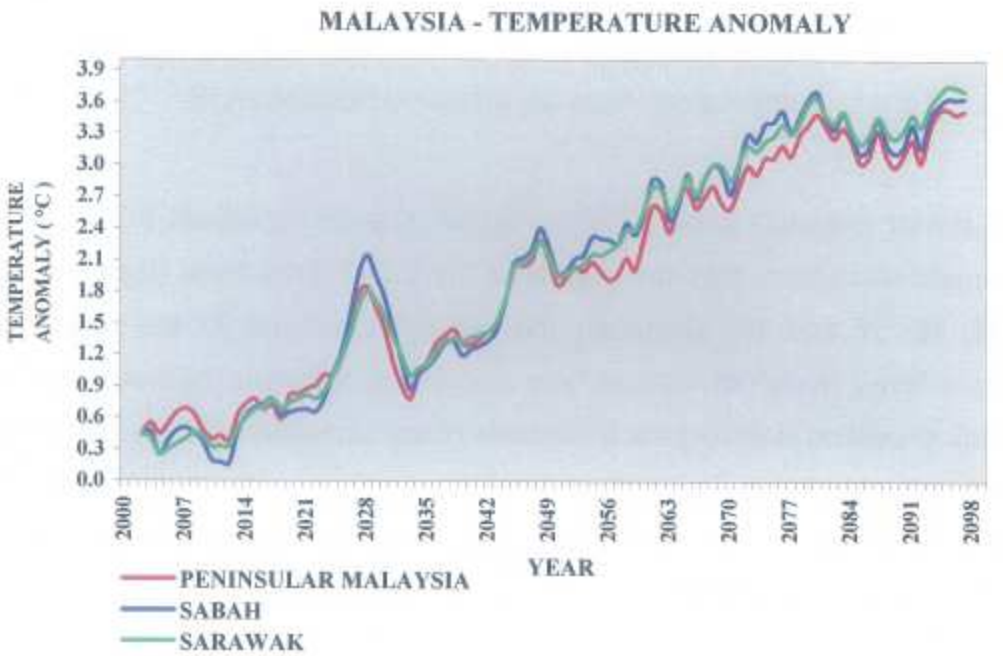

Figure 37: Precis Simulation (2001 – 2099) Annual Temperature Anomaly driven by HadCM3 A1B

Figures 37 to 41 display the annual and seasonal temperature anomaly trend for Peninsular Malaysia, Sabah and Sarawak. The general annual and seasonal temperature-increasing trend obtained is as expected with marked inter-decadal variability in the time-series. A significant reduction in annual average temperature simulation during the 8th decade (2080-2089) is noted.

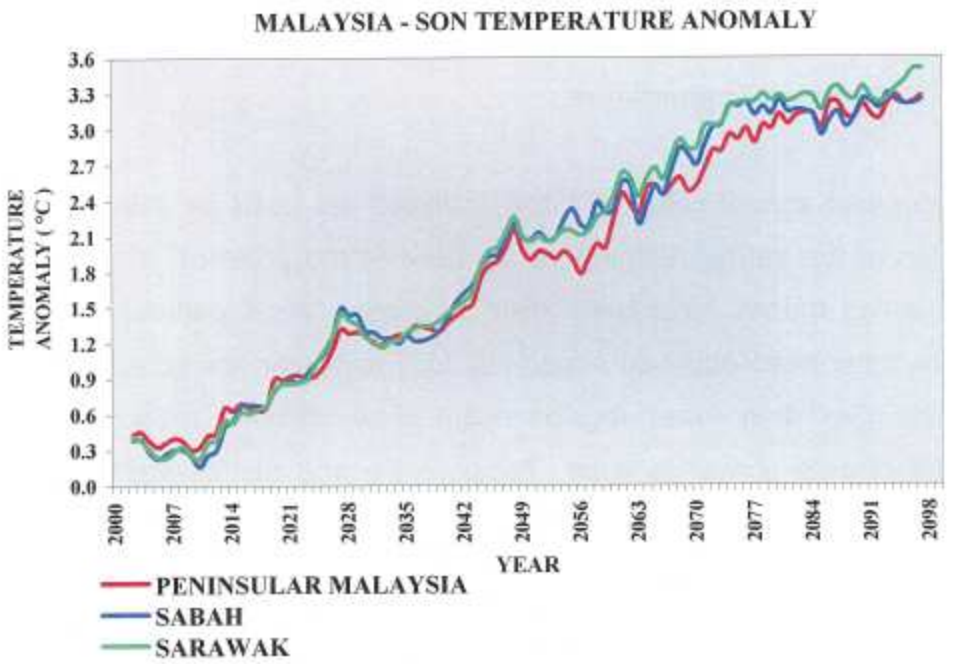

Figure 38: Precis Simulation (2001 – 2099) SON Temperature Anomaly driven by HadCM3 A1B

A similar reduction pattern is obtained for all seasons except SON. This RCM simulated pattern does not appear in the GCM simulations (**Figures 13**, **14**, **15**, **16**, **17** and **18**). Generally the temperature trend for the three regions considered does not indicate any significant departure between them. The only exception is during the 5th decade of the simulation (2050 –2059). During the decade, Peninsular Malaysia seems to show a temporary decrease in temperatures for JJA and SON, in contrast to the continually increasing temperatures of East Malaysia during the same period.

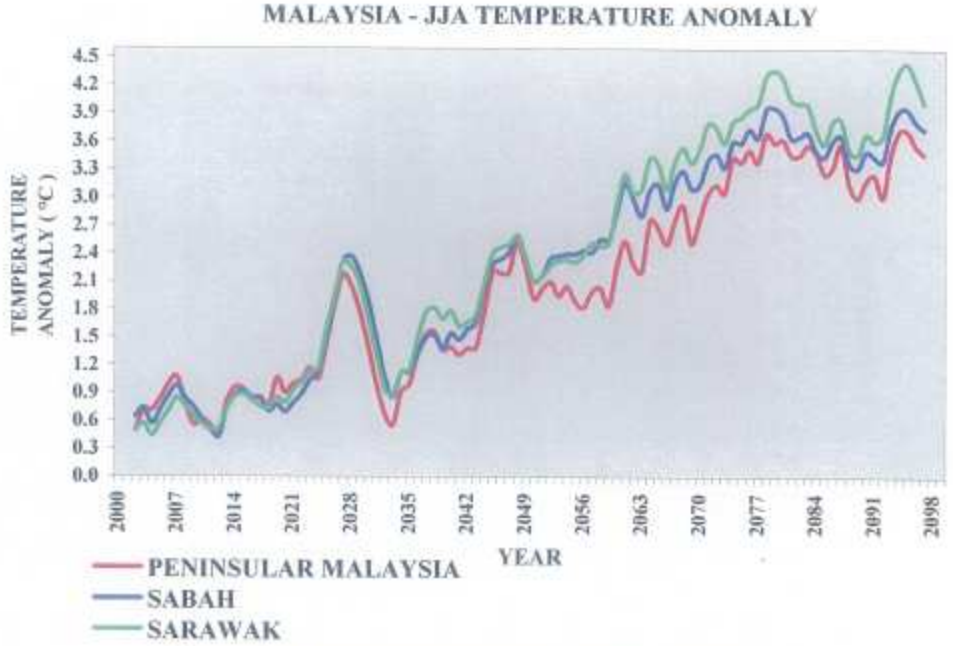

Figure 39: Precis Simulation (2001 – 2099) JJA Temperature Anomaly driven by HadCM3 A1B

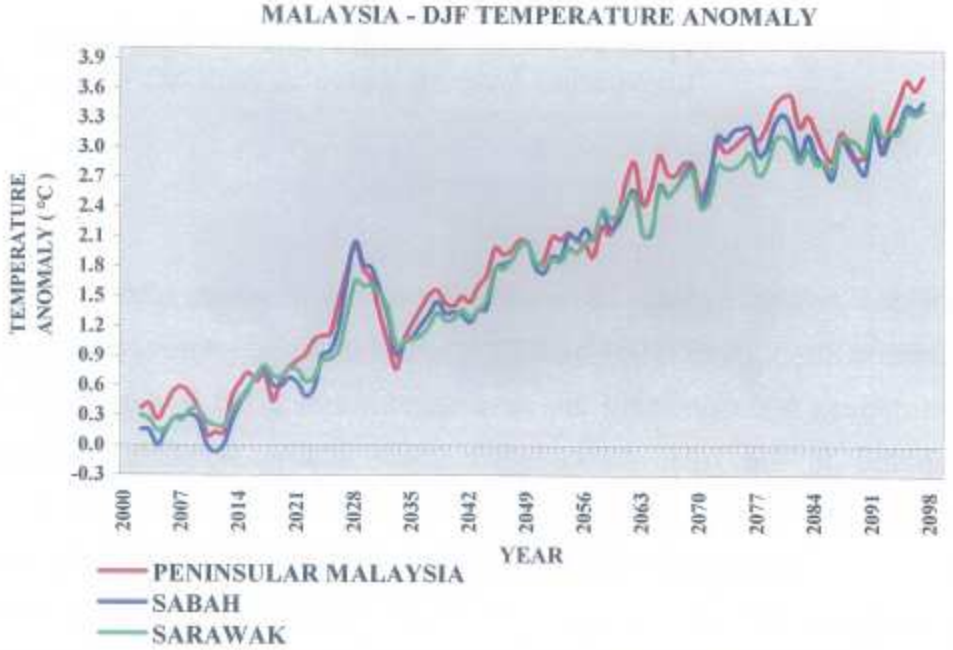

Figure 40: Precis Simulation (2001 – 2099) DJF Temperature Anomaly driven by HadCM3 A1B

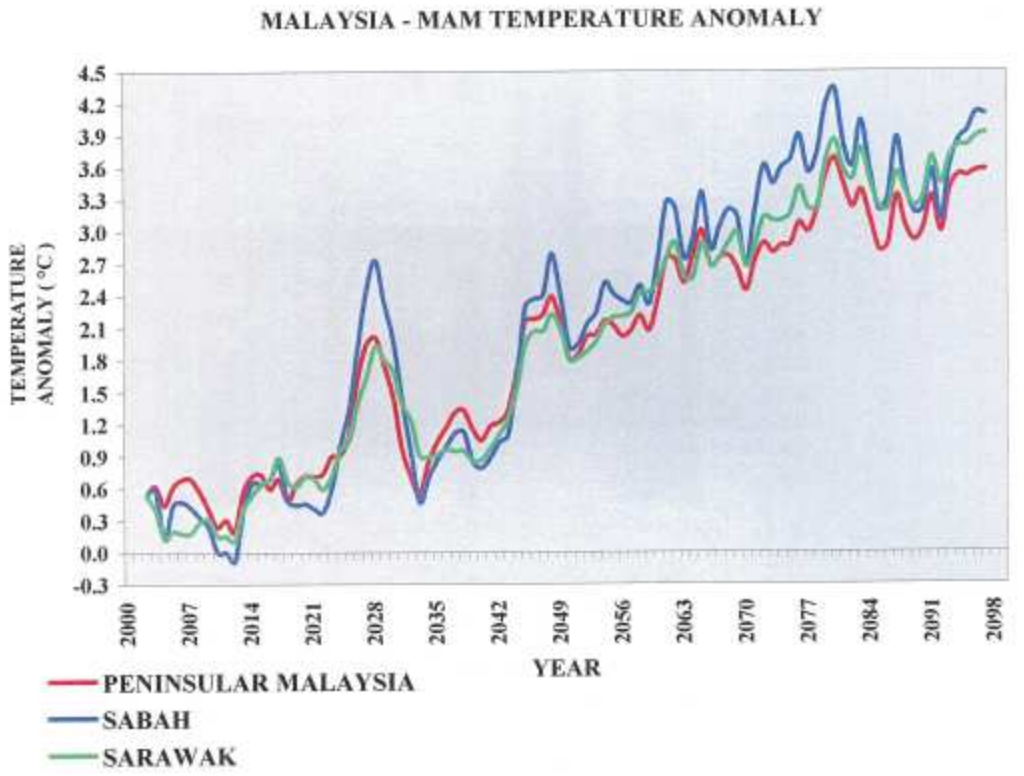

Figure 41: Precis Simulation (2001 – 2099) MAM Temperature Anomaly driven by HadCM3 A1B

Significant annual average temperature increase of record high temperatures for around 2028, 2048, 2061 and 2079 indicate strong interdecadel variability. Nevertheless the significant increase recorded in 2028 is extremely severe compared to the rest. All seasons show similar significant increase in temperatures during the four years mentioned above except for SON. Seasonal temperature increase is relatively similar among the three different regions for all the seasons except for MAM. During this season, temperature increase for Sabah is markedly higher compared to Sarawak and Peninsular Malaysia.

Highest and lowest temperature increase for Peninsular Malaysia is obtained during DJF (3.7°C) and SON (3.3°C) respectively. For Sabah the highest and lowest increase is obtained during MAM (4.1°C) and SON (3.2°C)

respectively. For Sarawak, the highest and lowest increase is obtained during MAM (3.9°C) and DJF (3.4°C).

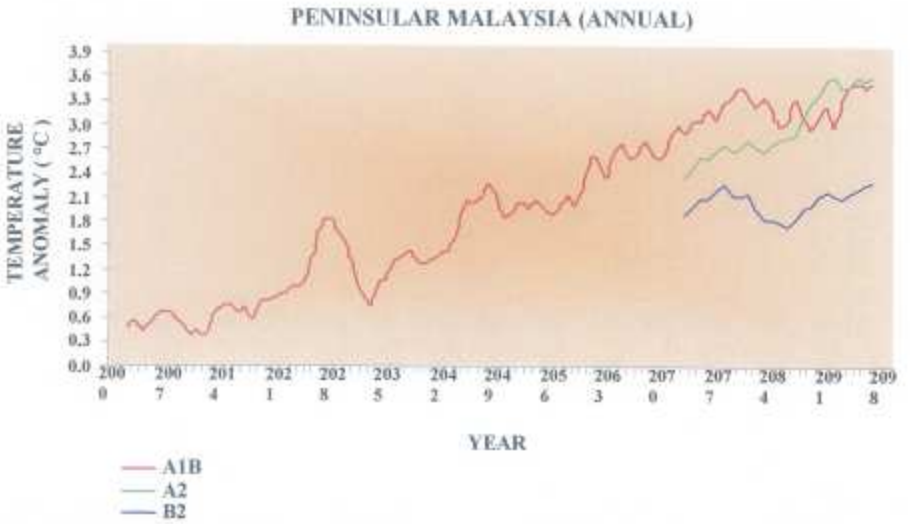

Figure 42: Precis Annual Temperature Anomaly Simulation for Peninsular Malaysia driven by HadCM3 A1B, HadAM3P A2 and B2

Figure 43: Precis Annual Temperature Anomaly Simulation for Sabah driven by HadCM3 A1B, HadAM3P A2 and B2

The A2 and B2 simulation results have been displayed together with the A1B simulation in **Figures 42**, **43** and **44**. Five-year running means were also obtained for the A2 and B2 simulations. As expected the temperature increase by the B2 simulation is less than that for the A2 simulation. The

temperature reduction obtained for the A1B simulation during 2080 – 2089 is also obtained for the B2 simulation, but not for the A2 simulation.

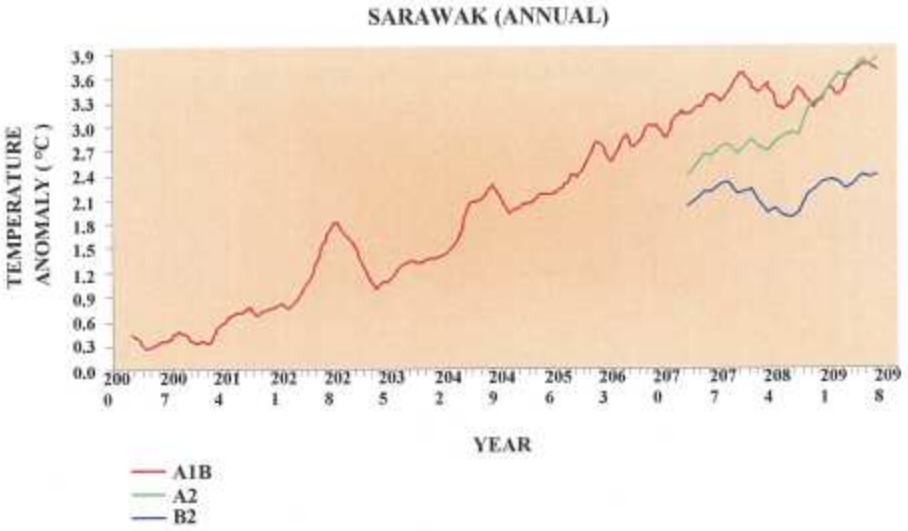

Figure 44: Precis Annual Temperature Anomaly Simulation for Sarawak driven by HadCM3 A1B, HadAM3P A2 and B2

Also the expected evident temperature increase for the A2 simulation over the A1B simulation is not obtained for all the three regions. Temperature increase for the A2 simulation is generally lower than that for the A1B simulation during the first half of the simulation period (2070 – 2085) and generally higher during the second half of the simulation period (2086-2099). Towards the last 5 to 7 years of the century the temperature increase indicated for the A2 simulation stabilizes to the 5 year running mean curve of the A1B simulation. This pattern is obtained for all three regions considered. For Peninsular Malaysia, the temperature increase range between the lowest value (indicated by the B2 simulation) and the highest value (indicated for the A2 simulation) is 2.3°C to 3.6°C. For Sabah and Sarawak the range is 2.4°C to 3.7°C.

Higher detailed regional analysis of PRECIS temperature simulations driven by the HadCM3 AOGCM, for three decades representing the first quarter (2020 – 2029), middle (2050 – 2059) and end of the century (2090 – 2099) relative to 1990-1999 period are displayed in **Table 2** and **Figures 45** and **46**.

Table 2: Annual Mean Temperature Changes (°C) relative to 1990-1999 period

Region	2020-2029	2050-2059	2090-2099
North-West PM	1.3	1.9	3.1
North-East PM	1.1	1.7	2.9
Central PM	1.5	2.0	3.2
Southern PM	1.4	1.9	3.2
East Sabah	1.0	1.7	2.8
West Sabah	1.2	1.9	3.0
East Sarawak	1.4	2.0	3.8
West Sarawak	1.2	2.0	3.4

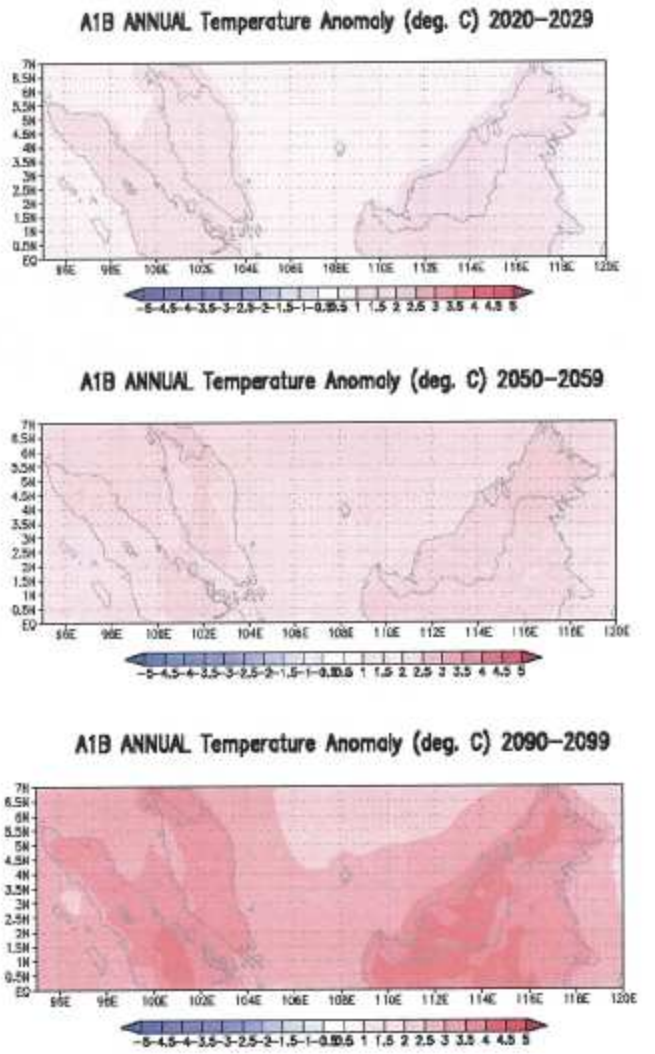

Figure 45: Annual Mean Temperature Anomaly Relative to 1990 - 1999

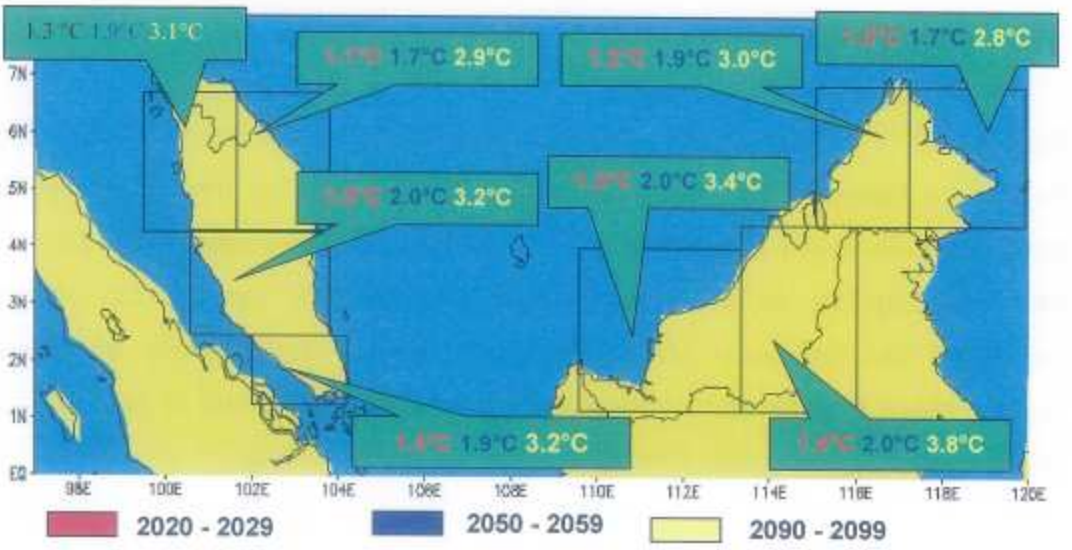

Figure 46: Annual Mean Temperature Anomaly Relative to 1990 - 1999

Generally higher temperatures are simulated for East Malaysia compared to Peninsular Malaysia. Higher temperature increase during the last decade is obtained for Sarawak compared to Peninsular Malaysia and Sabah. Eastern Sarawak region records the highest temperature increase (3.8°C) compared to North-eastern Peninsular Malaysia, which records the lowest (2.9°C). This is consistent with the simulation results in **Figure 37.** Central and Southern Peninsular Malaysia records higher simulated temperatures compared to Northern Peninsular Malaysia. The rate of temperature increase during the 30-year period from 2059 to 2090 is generally double the rate of increase simulated for earlier 20-year period from 2029 to 2050. Highest temperature increasing rate during the 60-year period from 2029 to 2090 is simulated for the Eastern Sarawak region (1.4°C to 3.8°C) compared to the lowest increase rate simulated for Central Peninsular Malaysia (1.5°C to 3.2°C).

4.4 Changes in Rainfall

Figures 47 to **51** display the annual and seasonal rainfall anomaly trend for Peninsular Malaysia, Sabah and Sarawak. The A2 and B2 simulation results have been displayed together with the A1B simulation in **Figures 52**, **53** and **54**. The negative annual rainfall trend is extremely evident for Sabah compared to Peninsular Malaysia and Sarawak. Nevertheless all three regions seem to experience increased rainfall towards the end of the century (2080 onwards), especially Peninsular Malaysia and Sarawak.

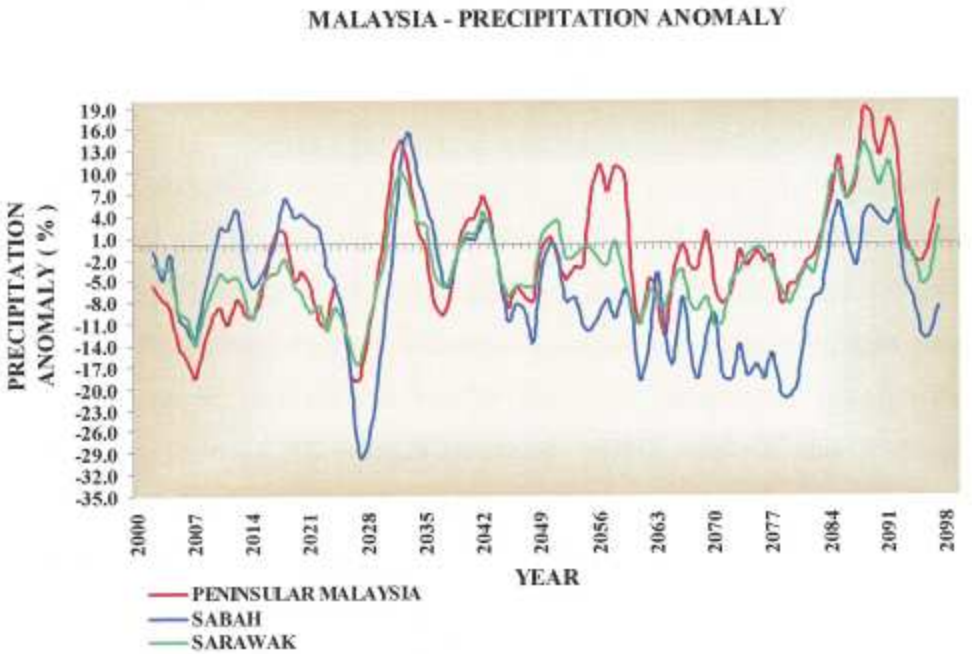

Figure 47: Precis Simulation (2001 – 2099) Annual Rainfall Anomaly driven by HadCM3 A1B

The significant increase in annual temperature simulated for 2028, 2048, 2061 and 2079 in **Figure 37** correspond to significant reduction in annual rainfall simulated for the same years in **Figure 47**. Of these years, highest rainfall reduction was simulated for 2028, which corresponds to the highest temperature increase simulated for annual temperature anomaly (**Figure 37**). This signal of significant reduction of rainfall together with significant increase in temperature is generally exhibited during El Niño events.

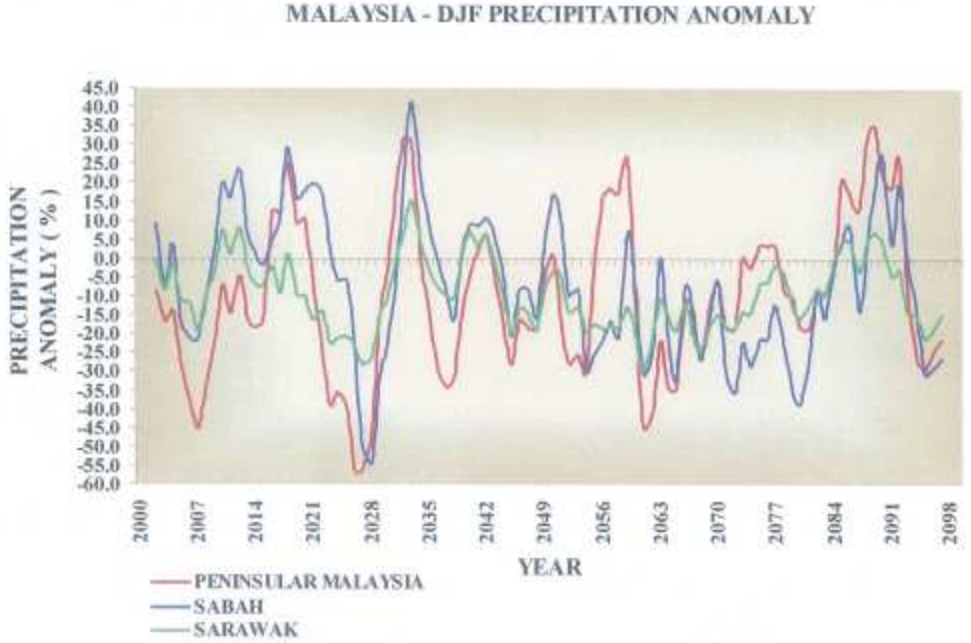

Figure 48: Precis Simulation (2001 – 2099) DJF Rainfall Anomaly driven by HadCM3 A1B

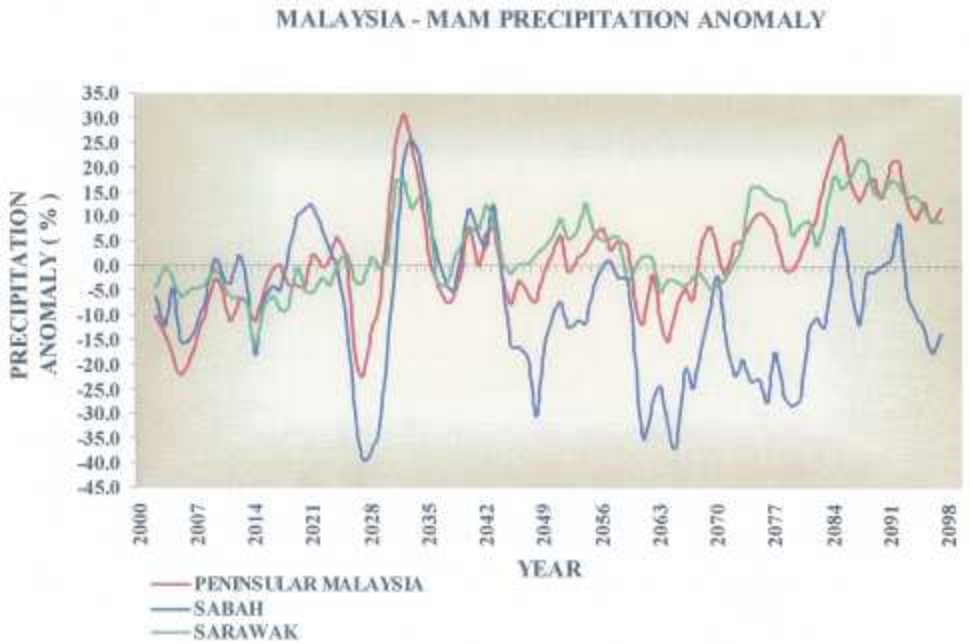

Figure 49: Precis Simulation (2001 – 2099) MAM Rainfall Anomaly driven by HadCM3 A1B

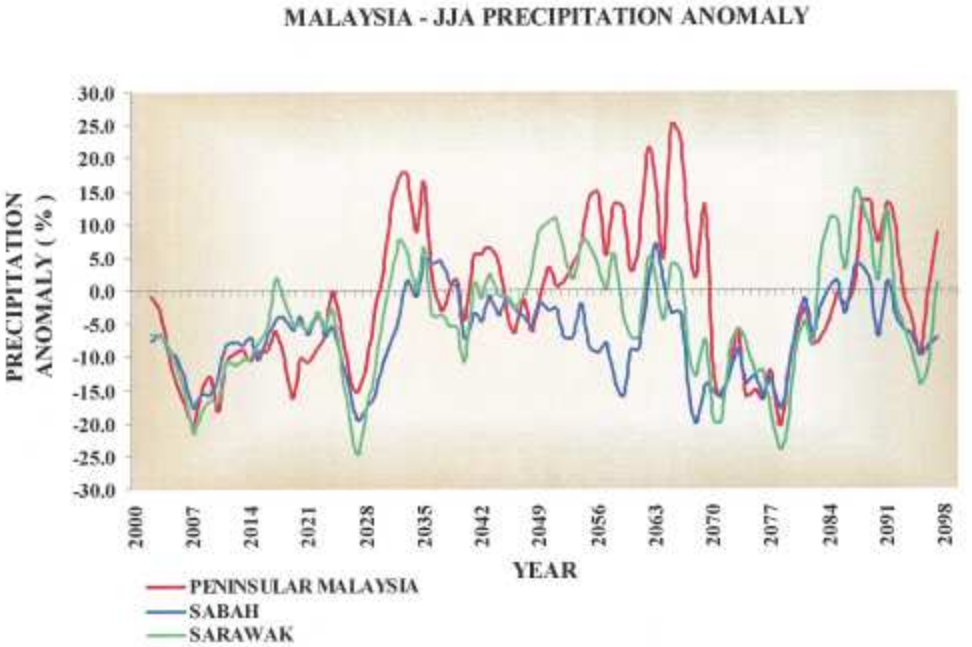

Figure 50: Precis Simulation (2001 – 2099) JJA Rainfall Anomaly driven by HadCM3 A1B

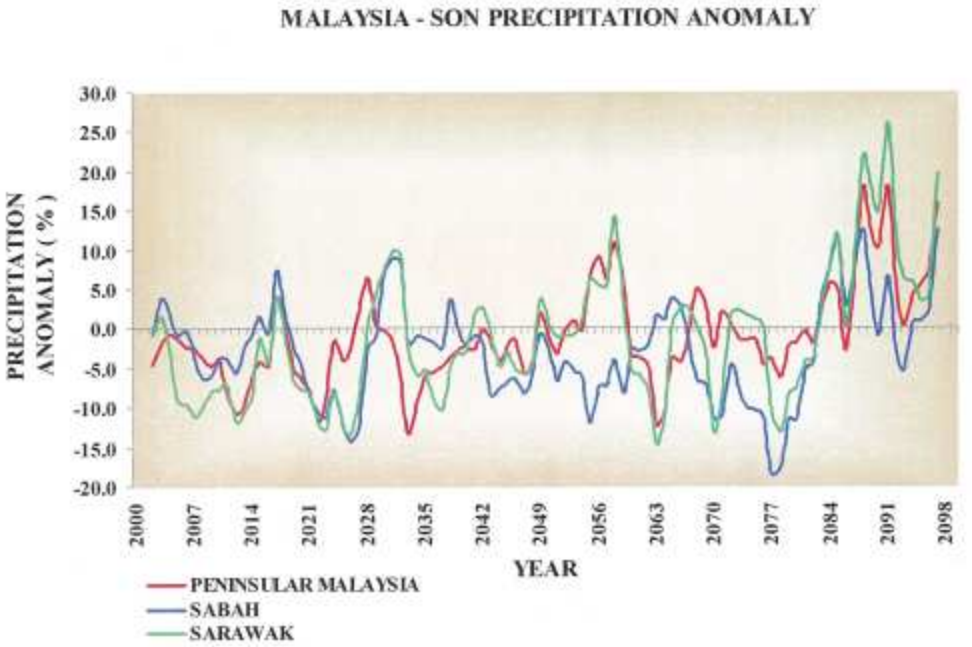

Figure 51: Precis Simulation (2001 – 2099) SON Temperature Anomaly driven by HadCM3 A1B

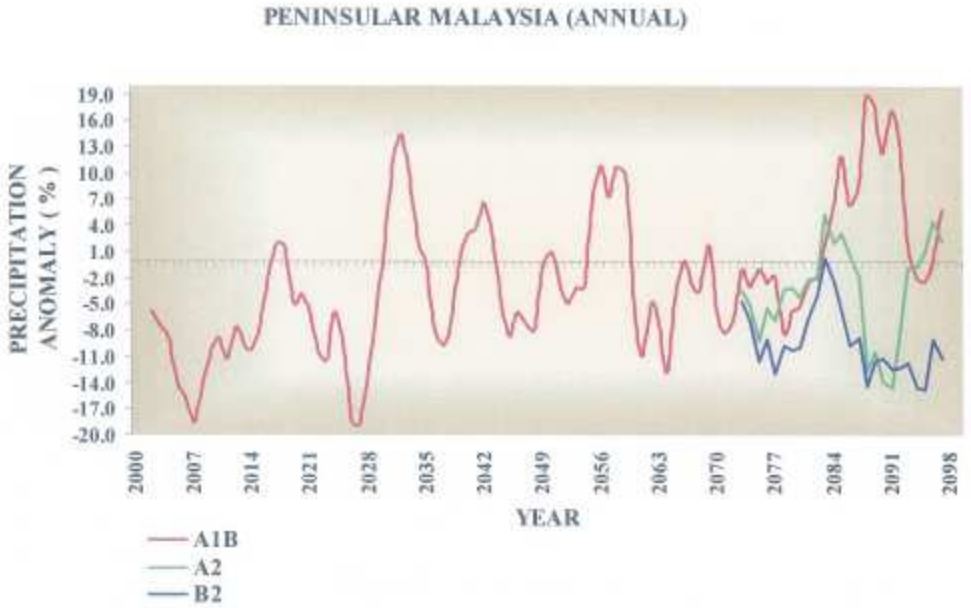

Figure 52: Precis Annual Rainfall Anomaly Simulation for Peninsular Malaysia driven by HadCM3 A1B, HadAM3P A2 and B2

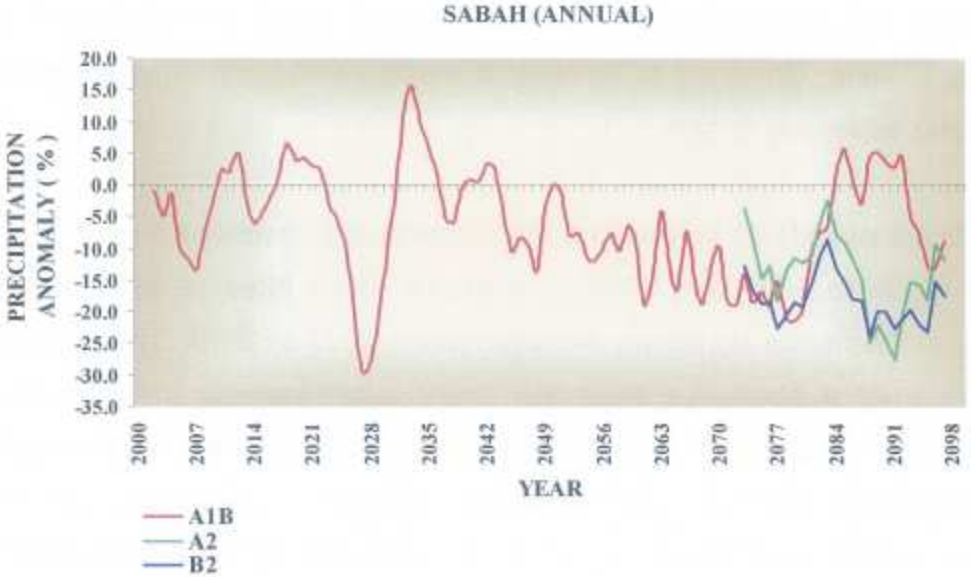

Figure 53: Precis Annual Rainfall Anomaly Simulation for Sabah driven by HadCM3 A1B, HadAM3P A2 and B2

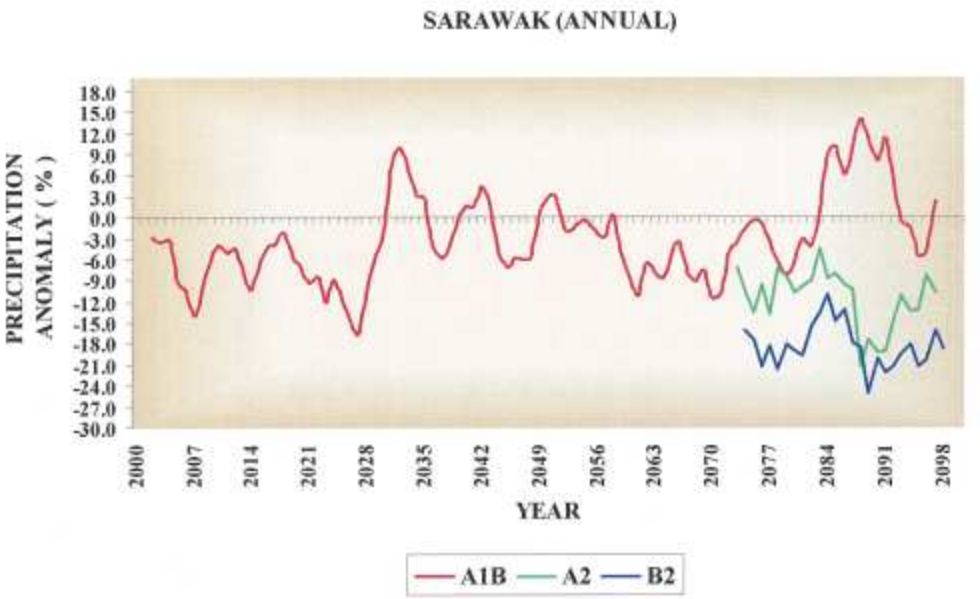

Figure 54: Precis Annual Rainfall Anomaly Simulation for Sarawak driven by HadCM3 A1B, HadAM3P A2 and B2

In the case of the four years mentioned above, all three regions Sabah, Sarawak and Peninsular Malaysia are affected, which is a signature of a strong El Niño. Generally an El Niño of mediocre strength only affects East Malaysia especially Sabah.

Significant periods of increased annual rainfall are simulated during 2030 to 2031, 2055 to 2058 and 2084 to 2091. Of these three periods, all three regions experience significant increase during 2030 to 2031. This bears the signature of a strong La Niña like event accompanying the supposedly simulated strong El Niño like event of 2028. During the two remaining simulated wet periods, only Peninsular Malaysia experiences significant annual rainfall increase during 2055 to 2058 and all regions experience significant annual increase in rainfall during 2084 to 2091. For the last 20 years of the simulated seasonal rainfall, increasing seasonal rainfall trend is obtained clearly for Sarawak and Peninsular Malaysia compared to Sabah for all the four seasons. The extremely significant reduction of rainfall during 2028 and the accompanying significant increase in 2030 t0 2031 mentioned above is captured clearly during all seasons except for SON.

Seasonal responses to rainfall simulated by the HadCM3 A1B scenario for Peninsular Malaysia, Sabah and Sarawak is displayed in **Figures 48**, **49**, **50** and **51**. During DJF, which is the period during which the regional rainfall variation is largest (-60% to 40%), significant variation between the most dry and wet periods is obtained for Peninsular Malaysia and Sabah. The DJF seasons for a 50-year span from 2035 to 2085 are relatively very dry for all regions. During MAM, Sabah seasonal rainfall is clearly much less compared to Peninsular Malaysia and Sarawak. During the last third of the simulation period (2065 – 2099), an upward trend of MAM seasonal rainfall seems to be established for all three regions. As of 2030, higher JJA seasonal rainfall is simulated for Peninsular Malaysia compared to Sabah and Sarawak. Variation of JJA seasonal simulated rainfall is largest for Sarawak compared to Peninsular Malaysia and Sabah. From 2050 to 2070, for the JJA simulated seasonal rainfall, the regional increased seasonal rainfall pattern obtained for Peninsular Malaysia is the longest continuous period of increased seasonal rainfall pattern obtained for all of the three regions and for all of the four seasons. The least variation in seasonal rainfall for all the regions is obtained during SON (-15% to 25%) as opposed to the highest during DJF.

The regional rainfall response to the A2, A1B and B2 scenarios are displayed in **Figures 52**, **53** and **54**. The 5-year running mean for the A2 and B2 annual rainfall has been simulated for the period from 2072 to 2097. Generally for all the three regions, less annual rainfall seems to be indicated for the B2 scenario compared to the A2 scenario. From around 2082 to 2093, very evidently an upward trend of annual rainfall is simulated for the A1B scenario, but a downward trend for both the A2 and B2 scenarios. Reduction in annual rainfall simulated in the A2 and B2 scenarios is more severe in Sabah and Sarawak compared to Peninsular Malaysia.

Higher detailed regional analysis of PRECIS rainfall simulations driven by the HadCM3 AOGCM, for three decades representing the first quarter (2020 – 2029), middle (2050 – 2059) and end of the century (2090 – 2099) relative to 1990-1999 are displayed in **Table 3** and **Figures 55** and **56**.

Table 3: Annual Rainfall Changes (%) relative to 1990-1999

Region	2020-2029	2050-2059	2090-2099
North-West PM	- 11.3	6.4	11.9
North-East PM	- 18.7	- 6.0	4.1
Central PM	- 10.2	2.3	14.1
Southern PM	- 14.6	- 0.2	15.2
East Sabah	- 17.5	- 12.8	- 3.6
West Sabah	- 8.9	- 1.2	0.3
East Sarawak	- 9.1	- 1.3	6.2
West Sarawak	- 8.8	3.8	14.6

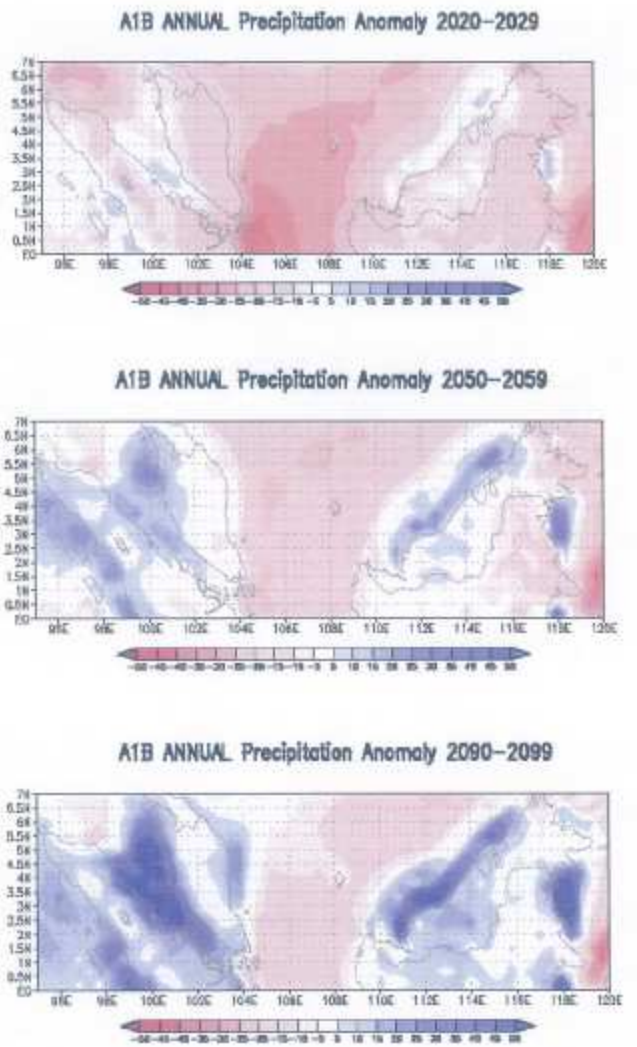

Figure 55: Annual Mean Rainfall Anomaly Relative to 1990 – 1999

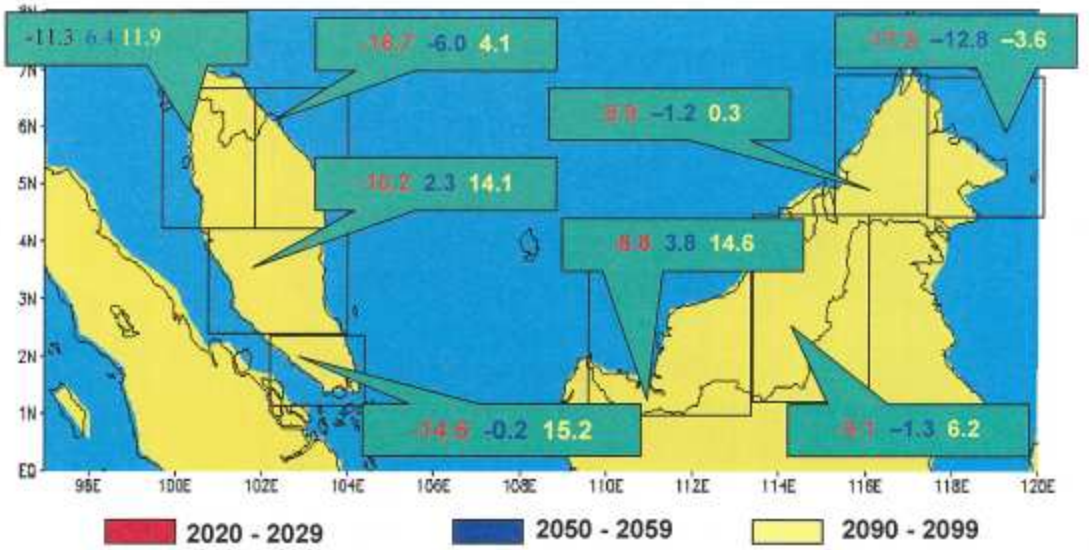

Figure 56: Annual Mean Rainfall Anomaly (%) Relative to 1990 – 1999

More rainfall is simulated during the last decade (2090 – 2099) for the whole country compared to the first quarter (2020 – 2029) and middle (2050 – 2059) of the century. Though rainfall amount seems to be increasing throughout Malaysia as the century progresses, nevertheless this is not the case as is shown by the annual anomalies for the three regions displayed in **Figure 47**. In actual fact from **Figure 47**, a negative anomaly for rainfall is simulated for Malaysia from the middle of the century until around 2080, after which rainfall for the whole country is simulated to increase. Higher amount of rainfall is simulated over land areas compared to the South China Sea. For all the three decades considered above, a negative anomaly is indicated for South China Sea.

Higher increase in rainfall is simulated for Peninsular Malaysia compared to East Malaysia during 2090 - 2099. During 2020 – 2029 it was the reverse with higher negative anomalies recorded in Peninsular Malaysia compared to East Malaysia, with the exception of East Sabah. Highest rainfall is simulated towards the end of the century for Southern Peninsular Malaysia, followed by Western Sarawak and Central Peninsular Malaysia. Least rainfall increase is simulated in Sabah with East Sabah recording a negative anomaly during 2090 – 2099 compared to the rest of the regions in Malaysia recording

positive anomalies during the same period. Least increase in rainfall is simulated for North-east Peninsular Malaysia compared to the rest of Peninsular Malaysia and Sarawak.

Chapter 5: Uncertainties in Climate Modelling

Uncertainties exist in each of the main stages required to provide climate change scenarios. It is necessary to consider these uncertainties when impacts, vulnerability and adaptation options are being assessed. Nevertheless it is very difficult to quantify all the aspects of these uncertainties. Some of the main source of uncertainties are future emission scenarios, future atmospheric greenhouse gas concentrations, incomplete understanding of global and regional climate system, pattern-scaling methods, natural variability and uncertainties in regional climate changes.

5.1 Future Emission Scenarios

Emission Scenario's uncertainty is identified as a major cause of uncertainty in projected future climates. Inherent uncertainties exist in the key assumptions in regard to relationships between future population, socio-economic development and technical changes, which form the base for the IPCC SRES Scenarios. Making climate projections for a range of SRES scenarios such as the presently available A1, A2, B1 and B2 emission scenario families can be one way to consider the uncertainties in emission scenarios. Moreover the uncertain nature of these emission paths has been well documented.

5.2 Uncertainties in Future Concentrations

Uncertainties in conversion of emission of greenhouse gases into atmospheric concentration result from incomplete understanding of the carbon cycle physics and chemical reaction processes in the atmosphere. Therefore this allows for a bigger potential uncertainty due to the feedbacks between climate, the carbon cycle and atmospheric chemistry. Added to the uncertainties above are uncertainties due to radiative forcing changes especially aerosol forcing associated with changes in atmospheric concentration. One particular example is the indirect cooling effect of sulphate aerosols on climate due to the modification of cloud properties.

One way to reflect these uncertainties are the usage of AOGCMs to explicitly simulate the carbon cycle and chemistry of all the substances required. Nevertheless this is seldom done and therefore these uncertainties are seldom reflected in the climate scenarios.

5.3 Climate Response Uncertainty

Much remains to be understood in regard to the workings of the climate system and therefore uncertainties arise due to the incorrect or incomplete description of key processes and feedbacks in the various GCMs. This is evident by the fact that current GCMs employing different representations of the climate system, project different patterns and magnitudes of climate change for the same period in the future using the same emission concentration scenarios.

Usage of a number of different GCMs as input to climate studies may be one way to reflect the various scientific uncertainties. Nevertheless the poor horizontal resolution of the ensemble might be source of further uncertainties. Common or systematic errors in simulation of current climate usually survive ensemble averaging and contribute error to the ensemble mean.

5.4 Uncertainties Due to Pattern-Scaling Methods

Pattern scaling methods were developed for equilibrium experiments performed with atmosphere only GCMs. Time slice emission scenarios such as the 2071 to 2100 simulation of the HadAM3P A2 and B2 emission scenarios involve the pattern scaling method. The climate change patterns for each time slice in the low emission, medium-low emission, medium-high emission and high emission scenarios are derived from a single master set of patterns. Although the patterns associated with each scenario and time slice are the same, the magnitudes are different. For each case, the master pattern is multiplied by the amount of global warming experienced at that time and for

the particular scenario. Scaling factors represents the amount of global warming experienced.

All pattern-scaling applications rely on three key assumptions. They are, firstly, the simulated anthropogenic climate change patterns are a function of global temperature. Secondly, the scaling patterns are independent of the history of greenhouse gas forcing, and finally the anthropogenic climate change signal can be adequately defined from climate model results. Herein lie the uncertainties associated with this method. Anthropogenic climate change patterns are not function of global temperature alone. Scaling patterns independent of greenhouse gas forcing history clearly does not incorporate radiative forcings due to greenhouse gas and aerosol concentration. Defining the anthropogenic climate change signal from climate model results cause the AGCM climate signal to inherit uncertainties already present in the source (AOGCM) itself.

5.5 Uncertainty Due to Natural Variability

The climate varies from timescales of years to decades due to natural interactions between the atmosphere, ocean and land. For a given period in the future natural variability could either reinforce the underlying human-induced change or could counteract it. This uncertainty cannot be removed but can be quantified by running ensembles of future climate projections. Each member of the ensemble uses the same GCM and the same emission scenario. The difference between each member is their different initial conditions. A range of the possible futures for a particular decade or decades together will be the result of the ensemble.

5.6 Uncertainty in Regionalization of Climate Change

Naturally all regionalization techniques carry with them any errors in the driving GCM fields. Uncertainties arising during dynamic downscaling are due to imperfect representation of physical processes, limitations due to numerical approximations of regional model equations and internal model variability.

Other than the RCM itself, the internal variability of the global and regional climate systems adds another level of uncertainty to regional climate change simulation. Therefore different regionalization techniques can give rise to different local projections even when based upon the same GCM.

5.7 Discussion

The inability of regional climate models to predict regular periodic ocean-atmospheric oscillations such as the El Niño, La Niña and the Indian Ocean Dipole (IOD) is another source of uncertainty in regard to RCM projections. Nevertheless it has to be understood that the RCM will only be able to simulate these oscillations if their signal had earlier been simulated in the AOGCM simulations.

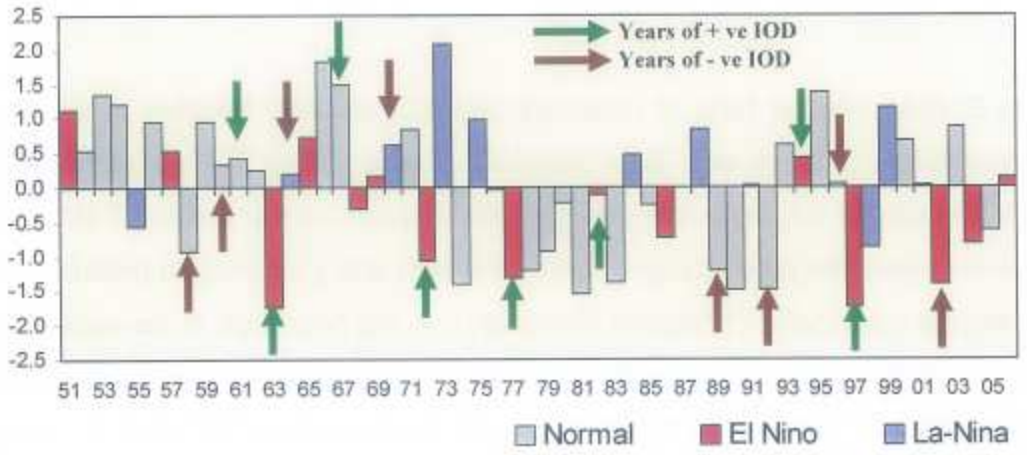

Figure 57: Standardized Annual Precipitation Anomaly for Peninsular Malaysia

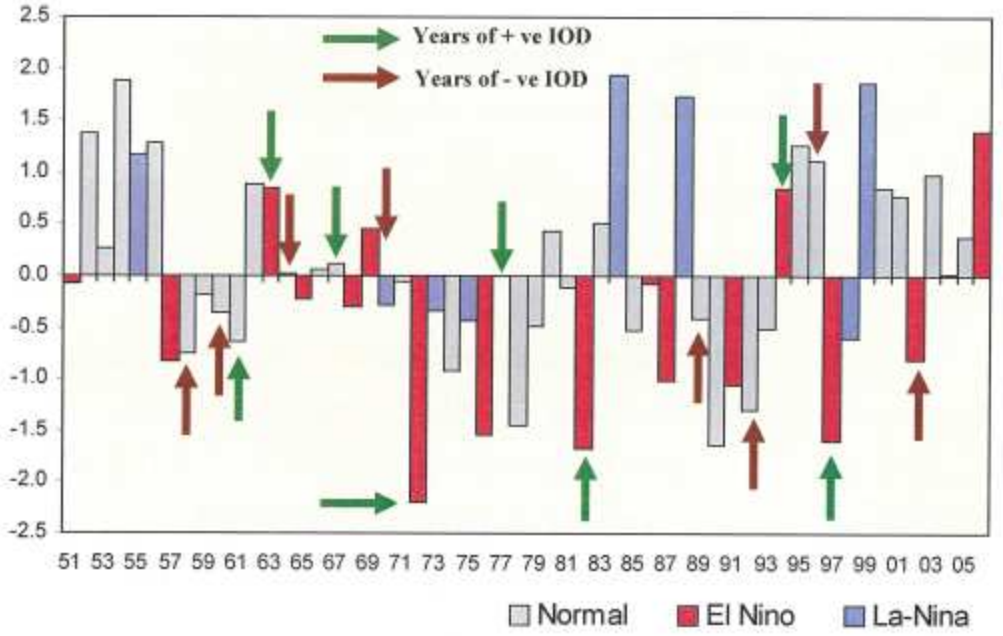

Figure 58: Standardized Annual Precipitation Anomaly for East Malaysia

An El Niño and La Niña of mediocre strength will only be able to influence precipitation patterns over East Malaysia. But a strong El Niño and La Niña will be able to influence the precipitation patterns of the whole of Malaysia. Nevertheless the relationship between the IOD and precipitation patterns over Malaysia (especially Peninsular Malaysia) has not been able to be established yet. Naturally an IOD of negative phase corresponds to warmer sea surface temperatures over eastern Indian Ocean compared to the positive phase, which correspond to a colder sea surface temperature over the eastern Indian Ocean. Therefore it is difficult to come up with any correlation between the IOD and ENSO (Ashok et al 2003).

From **Figures 57 and 58**, it can be seen that most of the severe El Niño events had contributed to significant annual reduction in precipitation to both Peninsular Malaysia and East Malaysia. These significant reductions in annual precipitation were recorded during 1963, 1972, 1977, 1986, 1997 and 2002. Nevertheless not all relatively significant reduction in annual precipitation years especially for Peninsular Malaysia correlated to the

presence of the El Niño event. Though the three most significant reductions in annual precipitation for East Malaysia (1972, 1982 and 1997) had correlated to a severe El Nino and a positive IOD event, the relationship ends there. In 2002, when another El Niño event was present, there was significant reduction in annual precipitation throughout Malaysia. But this El Niño event was accompanied by a negative IOD event. The three wettest years for East Malaysia were recorded during the La Niña years (1984, 1989 and 1999). Neither the negative phase nor the positive phase of the IOD was present during these three years. Similarly during the La Niña events, increase in annual precipitation was observed for Peninsular Malaysia, but neither the positive phase nor the negative phase of the IOD present. Also not all the significant wet years for Peninsular Malaysia had occurred during the La Niña event. Therefore trying to correlate completely the extreme precipitation patterns across Peninsular Malaysia and East Malaysia with either the El Niño, La Niña or IOD or a combination of them is futile.

Therefore given our incomplete understanding of the regional climate and global climate it will be difficult to remove the inherited uncertainties of the global and regional simulations. Evidently climate models may not be totally successful to simulate severe future extreme events given that the El Niño and La Niña events were important for the observation of extreme events. Further research also needs to be done to consider relevance of other large-scale climate signals such as the Madden Julian Oscillation (MJO) and Pacific decadal Oscillation (PDO) towards global and regional climate simulations.

Bibliography and Literature Sources

Aldhous, P. (2004) Borneo is burning, *Nature* **432**, 144-146

Ashok, K., Guan, Z. and Yamagata, T., (2003) A look at the relationship between the ENSO and the Indian Ocean Dipole, *J. Met. Soc. Japan* **81**, 41 - 56

Chan, J.C.L. and Li, C.Y., (2004) East Asian Winter Monsoon. *World Scientific Series on Meteorology of East Asia* Volume **2**, 54 - 106

Collins, M., Tett, S.F.B. and Cooper, C. (2001) The Internal climate variability of HadCM3, a version of the Hadley Centre coupled model without flux adjustment, *Climate Dynamics* **17**, 61 - 81

Cruz, R.V.O., Lasco, R.D., Pulhin, J.M., Pulhin, F.B. and Garcia, K.B. (2006) Climate change impact on water resources in Pantabangan Watershed, Philippines, *AIACC Final Technical Report*, 9-107

Fan, D.D. and Li, C.X. (2005) Complexities of Chinese coast in response to climate change, *Advance in Research on Climate Change* **1**, 111-114

Giorgi, F., Hewitson, B., Christensen, J., Fu, C., Jones, R., Hulme, M., Mearns, L., Storch, H. V. and Whetton, P., (2001) Regional Climate Information – evaluation and projections. Chapter 10 of: *Climate Change 2001: The Scientific Basis*. Contribution of Working Group1 to the Third Assessment Report of the Intergovernmental Panel on Climate Change

Hori, M. E. and Ueda, H., (2006) Impact of global warming on the East Asian Winter Monsoon as revealed by nine coupled atmosphere-ocean GCMs *Geophys. Res. Lett.* **L03713**

Hulme, M. and Jenkins, G.J. (1998) *Climate Change Scenarios for the UK Scientific Report: UKCIP Technical Report No 1,* Climatic Research Unit, Norwich, UK, 80pp

Hulme, M., Jenkins, G.J., Lu, X., Turnpenny, J.R., Mitchell, T.D., Jones, R.G., Lowe, J., Murphy, J.M., Hassell, D., Boorman, P., Mcdonald, R. and Hill, S. (2002) *Climate Change Scenarios for the United Kingdom: The UKCIP02 Scientific Report,* Tyndall Centre for Climate Research, School of Environmental Sciences, University of East Anglia, Norwich, UK.

IPCC (2000) Special Report on Emission Scenarios (SRES): Special Report of Working Group III of IPCC, Cambridge University Press, Cambridge, UK, 599pp

IPCC (2007) Summary for Policymakers (SPM) Report of Working Group1

IPCC (2007) Working Group 2 Report "Impacts, Adaptation and Vulnerability" Johns, T.C., Ingram, W.J., Johnson, C.E., Jones, A., Mitchell, J.F.B., Roberts, D.L., Sexton, D.M.H., Stevenson, D.S., Tett, S.F.B. and Woodage, M.J. (2001) Anthropogenic climate change for 1860 to 2100 simulated with the HadCM3 model under updated emissions scenarios *Hadley Centre Technical Note 22*

Jones, P.D., New, M., Parker, D.E., Martin, S. and Rigor, I.G. (1999) Surface air temperatures and its changes over the past 150 years *Reviews Geophysics* **37**, 173 – 199

Mearns, L. O., Hulme, M., Carter, T. R., Leemans, R., Lal, M. and Wheeton, P., (2001) Climate Scenarios Development *Climate Change 2001: The Scientific Basis.* Contribution of Working Group I to the Third Assessment Report of the Intergovernmental Panel on Climate Change

Morita, T., Robinson, J., Adegbulugbe, A., Alcamo, J., Herbert, D., Rovere, E. L. L., Nakicenovic, N., Pitcher, H., Raskin, P., Riahi, K., Sankovski, A., Sokolov, V., Vries, D. D. and Zhou, D., (2001) Greenhouse Gas Emission Mitigation Scenarios and Implications *Climate Change 2001: Mitigation* Contribution of Working Group III to the Third Assessment Report of the Intergovernmental Panel on Climate Change

Murdiyarso, D. and Adiningsih E. (2006) Climatic anomalies, Indonesian vegetation fires and terrestrial carbon emissions *Mitigation and Adaptation Strategies for Global Change* **12**, 101-112

Page, S.E., Siegert F., Rieley, J.O., Boehm, H.D.V. and Jaya, A. (2002) The amount of carbon released from peat and forest fires in Indonesia during 1997 *Nature* **420**, 61-65

Scott, P.A., Tett, S.F.B., Jones, G.S., Allen, M.R., Mitchell, J.F.B. and Jenkins, G.J. (2000) External control of twentieth century temperature by natural and anthropogenic forcings *Science* **15**, 2133 – 2137

Saji, N. H., Goswami, B. N., Vinayachandran, P. N. and Yamagata, T., (1999) A dipole mode in the Tropical Indian Ocean, *Nature* **401**, 360 - 363

Tran, V.L., Hoang, D.C. and Tran, T.T. (2005) Building of climate change scenario for Red River catchments for sustainable development and environmental protection. Preprints, *Science Workshop on Hydrometeorological Change in Vietnam and Sustainable Development*, Hanoi, Vietnam, Ministry of Natural Resource and Environment, 70-82

Trenberth, K.E. and Hoar, T.J. (1997) El Niño and climate change *Geophys. Res. Lett.* **24**, 3057-3060

Wigley, T.M.L. and Raper, S.C.B. (2001) Interpretation of high projections for global- mean warming *Science* **293**, 451 - 454

Zhang, C. (2005) Madden-Julian Oscillation *Reviews of Geophysics* **43**, 1 - 36

Zhou, W., Wang, X., Zhou, C. L. and Chan, J. C. L., (2007) Interdecadal Variability of the Relationship Between the East Asian Winter Monsoon and ENSO *Meteorol Atmos Phys* **98**, 283-293

Appendix 1: SRES Emission Scenarios

Emission scenarios describe how greenhouse gases emissions could evolve between 2000 and 2100, depending on various hypotheses. Such scenarios are indispensable to compare between them the results of the various climate models. Each of them reflects a plausible state of the future world, meaning that it is not possible today, to state that one of them is incompatible with the information that we have, even if some of them might seem "extreme".

The IPCC has described 40 scenarios grouped into 4 main families' marker scenarios. Each family, named by an abbreviation (A1, A2, B1 and B2) reflects a particular evolution of humanity which have different characteristics in regard to population growth, economic activity, technology spreading etc.

Storyline	Description
A1	Rapid economic growth; Population peaks at 9 billion at mid century; Efficient technology spreading; Social, cultural and economic convergence among regions; Three mixes of energy variants: **A1F1** – reliance on fossil fuel; **A1T** – reliance on non-fossil fuel; **A1B** – balance between fossil and non-fossil fuel.
A2	Different economic growth rate and efficiency of technology dependent upon regional scales; Population reaching 15 billion in 2100 and increasing.
B1	Population peaks at 9 billion at mid century; Efficient technology spreading; Global solutions to economic, social and environmental sustainability.
B2	Population reaches 10 billion in 2100 (slower rate than A2) and increasing; Local solutions to sustainability; Development and spread of technology is uneven and slower than for A1 or B1.

ISBN 978-983-99679-1-3

Dicetak Oleh : Unit Percetakan, Jabatan Meteorologi Malaysia
Jalan Sultan, 46667 Petaling Jaya